Access-Backhaul Strategy via gNB Cooperation for Integrated Terrestrial-Satellite Networks

Girim Kwon, *Member, IEEE*, Wonjae Shin, *Senior Member, IEEE*, Andrea Conti, *Fellow, IEEE*, William C. Lindsey, *Life Fellow, IEEE*, and Moe Z. Win, *Fellow, IEEE*

***Abstract*— Integrated terrestrial-satellite networks (ITSNs) play an essential role in providing global and ubiquitous connectivity for next generation networks. Spectral efficiency of ITSNs depends on their integrated architecture and the operational strategies, including interference management and resource allocation. This paper proposes an efficient integrated access and backhaul (IAB) architecture for terrestrial-satellite networks considering both uplink (UL) and downlink (DL) communications. We aim to integrate terrestrial access and satellite backhaul networks by developing a novel optimization framework for their joint operation. In particular, in-band access-backhaul transmission is considered for high spectral efficiency, where a reverse time division duplexing is used to prevent both self-interference and interference between access links and backhaul links. In addition, cooperation among gNodeB is taken into account to overcome harsh propagation conditions such as blockage effects and severe pathloss. A framework for joint optimization of cooperative beamforming and resource allocation is developed to maximize the UL-DL rate region of the in-band IAB. The proposed architecture is verified using the 3rd Generation Partnership Project (3GPP) channel models. Numerical results show that the proposed architecture significantly outperforms the classical out-of-band backhauling while approaching an outer bound of the UL-DL rate region.**

***Index Terms*— Integrated terrestrial-satellite networks, integrated access and backhaul, cooperative beamforming, reverse time division duplexing, next generation networks.**

I. Introduction

NON-TERRESTRIAL NETWORKS are expected to play a key role in vertical domain expansion of next generation mobile communications and have been under exploration in the 3rd Generation Partnership Project (3GPP) [1], [2], [3], [4], [5]. Non-terrestrial networks are crucial to support global broadband coverage for ubiquitous connectivity, which is one of six key usage scenarios defined in IMT-2030 (6G) [6], [7], [8]. Enabling techniques for the ubiquitous connectivity include the advanced backhaul connections and the integrated terrestrial-satellite networks (ITSNs) employing satellites or space-air vehicles [9], [10], [11], [12], [13], [14], [15], [16]. In particular, high-throughput satellites can be exploited for global broadband services in the form of ITSNs.

The integrated design of terrestrial-satellite networks (TSNs) has been studied in different forms from the perspectives of ubiquitous connectivity and enhanced throughput. In [17], [18], [19], and [20], a terrestrial relay is used between a satellite and a user equipment (UE) so that the UE can communicate with the satellite even when the direct link between them has a poor quality. In [21], [22], [23], [24], and [25], the coexistence of terrestrial UE and satellite UE has been investigated, where interference between terrestrial networks and satellite networks is efficiently mitigated by robust interference management schemes. In [26] and [27], cooperative transmission between terrestrial base stations and satellites has been considered to provide diversity gain in TSNs. While most of previous works have considered satellite networks as direct access networks for UEs, establishing advanced backhaul links between the core network and the base stations in remote areas is needed from the perspective of global broadband coverage.

Integrated access and backhaul (IAB) architecture is vital for providing global broadband coverage by combining terrestrial access networks with satellite backhauls, particularly for urban hotspots, disaster areas, and isolated rural areas [28], [29], [30], [31], [32]. For example, TSNs with IAB can achieve a higher capacity than direct satellite access by exploiting high transmit power and beamforming (BF) gain of terrestrial gNodeBs (gNBs). In addition, the use of satellite backhaul can benefit from flexible and cost-effective network operation, especially in the challenging areas compared to the terrestrial infrastructure-based backhaul. The main challenges in designing TSNs with IAB are: to establish reliable satellite networks [32], [33], [34]; and to optimize the integrated network operation for capacity maximization [31].

To establish satellite networks with global broadband coverage, advanced geostationary orbit (GEO) satellite constellations are expected. For example, Viasat's *ViaSat-3* constellation consisting of three high-throughput satellites is planned to provide up to 100 Mbps services on *Ka*-band and

Manuscript received 30 July 2023; revised 15 November 2023; accepted 18 December 2023. Date of publication 14 February 2024; date of current version 9 May 2024. The fundamental research described in this paper was supported, in part, by the National Research Foundation of Korea under Grant 2021R1A6A3A14040142 and Grant 2022R1A2C4002065, by the Office of Naval Research under Grant N62909-22-1-2009, by the National Science Foundation under Grant CNS-2148251, and by federal agency and industry partners in the RINGS Program. The material in this paper was presented in part at the IEEE International Conference on Communications, Rome, Italy, May 2023. *(Corresponding author: Wonjae Shin.)*

Girim Kwon is with the Wireless Information and Network Sciences Laboratory, Massachusetts Institute of Technology, Cambridge, MA 02139 USA (e-mail: girimk@mit.edu).

Wonjae Shin is with the School of Electrical Engineering, Korea University, Seongbuk-gu, Seoul 02841, South Korea (e-mail: wjshin@korea.ac.kr).

Andrea Conti is with the Department of Engineering and CNIT, University of Ferrara, 44122 Ferrara, Italy (e-mail: a.conti@ieee.org).

William C. Lindsey is with the Ming Hsieh Department of Electrical Engineering, University of Southern California, Los Angeles, CA 90089 USA (e-mail: wclindsey@gmail.com).

Moe Z. Win is with the Laboratory for Information and Decision Systems (LIDS), Massachusetts Institute of Technology, Cambridge, MA 02139 USA (e-mail: moewin@mit.edu).

Color versions of one or more figures in this article are available at https://doi.org/10.1109/JSAC.2024.3365877.

Digital Object Identifier 10.1109/JSAC.2024.3365877

a total capacity of at least 1 Tbps per satellite starting from 2023. In addition, Inmarsat's *Inmarsat-6* satellites are anticipated to support both *L*-band and *Ka*-band with independent beams that can be reconfigured across the globe. Meanwhile, localization error outage (LEO) satellite constellations are also being formed in the industry (e.g., SpaceX, Amazon, OneWeb, Telesat, and Boeing). In tandem with the efforts to set up the satellite constellations, optimization techniques for integrating the satellite backhaul and terrestrial access networks are also required.

Wireless backhauling has received increasing attention in the area of terrestrial networks due to easy installation and flexible operation, which has been standardized under the name of IAB in fifth generation (5G) New Radio (NR) [35]. The research on wireless backhaul systems has been conducted in two main streams, i.e., out-of-band backhauling and in-band backhauling, respectively depending on whether the frequency band is separated or shared between the backhaul and the access network. The works in [36], [37], [38], [39], [40], [41], and [42] have considered out-of-band backhauling to avoid interference between access and backhaul links. They have mainly focused on bandwidth allocation and interference mitigation within access links or backhaul links. On the other hand, the works on in-band wireless backhauling have studied interference management for sharing the spectrum between access and backhaul links [43], [44], [45], [46]. It has been shown that in-band backhauling with interference mitigation techniques is more resource-efficient than out-of-band backhauling in IAB networks [43], [44]. Most of the works have focused on BF design for downlink (DL) transmission assuming the base station-centric user association in the access networks. To enable global broadband connectivity, a BF scheme for spectrally efficient TSNs with in-band IAB is needed.

BF designs for TSNs have been actively studied in recent years [47], [48], [49], [50], [51], [52], [53], [54], [55]. The works in [47], [48], and [49] have designed multi-user BF schemes for the satellite communication systems without consideration of coexistence or integration with terrestrial networks. The works in [50], [51], [52], [53], and [54] have considered coexistence of the satellite access network and terrestrial access network, where they have designed BF schemes for satellite and/or terrestrial base stations in the presence of interference between the satellite and base stations. These works have considered the satellite as a separate base station serving UEs rather than as a wireless backhaul. The work in [55] designed a BF scheme for the in-band IAB in TSNs with an earth station, which relays the satellite signal to a separate base station. However, it only considered the DL transmission with a single base station. For spectrally efficient in-band IAB, joint optimization of BF and resource allocation is needed in the TSNs that accounts for both uplink (UL) and DL characteristics. Moreover, cooperative BF of multiple gNBs is vital in TSNs to overcome the high pathloss and blockage effect in non-terrestrial channels by exploiting macro-diversity [56], [57].

The fundamental questions related to the TSN with IAB are the following.

- How to design an efficient architecture of IAB for TSNs that provides high spectral efficiency?
- How to jointly optimize BF and resource allocation that maximize the UL-DL rate region?

The answers to these questions will enable the ubiquitous connectivity based on the satellites that are planned to be launched in the foreseeable future. The goals of this paper are to establish an efficient in-band IAB architecture for TSNs and show the gain over the conventional backhauling. We aim to develop a framework for joint optimization of cooperative BF and resource allocation. We advocate the use of reverse time division duplexing (TDD)-based IAB so that the uplink and downlink transmission are in a reversed order at the satellite backhaul links and the terrestrial access links. This enables spectrally efficient TSNs for the efficient integration of the satellite and terrestrial resources.

This paper explores the design of an ITSN with terrestrial access and satellite backhaul considering both UL and DL transmissions. The key contributions of this paper are summarized as in the following.

- We propose an in-band IAB architecture for spectrally-efficient TSNs based on reverse TDD, enabling to avoid potential self-interference and interference between access and backhaul links. Cooperative BF of gNBs is taken into account to overcome harsh propagation conditions such as blockage and pathloss.
- We develop a framework for joint optimization of BF and of resource allocation to enlarge the UL-DL rate region of the ITSN. Specifically, we reformulate the joint optimization problem into a bilevel optimization form where a lower-level problem is nested within an upper-level problem to design efficient algorithms.
- We design a cooperative BF and resource allocation algorithm based on our optimization framework for maximizing the weighted sum of end-to-end UL and DL rates. We derive the necessary conditions of optimality, and find the best solution via iterative algorithms.
- We quantify the performance gain of the proposed in-band IAB architecture over conventional in-band and out-of-band backhaul schemes for 3GPP non-terrestrial and terrestrial channel models. The proposed architecture achieves a larger area of the UL-DL rate region compared to benchmark schemes, while approaching the outer bound of the rate region.

The remaining sections are organized as in the following: Sec. II introduces the system model of the proposed ITSN. Sec. III describes the optimization framework. Sec. IV presents the design of the proposed algorithms. Sec. V provides the simulation results. Finally, Sec. VI gives our conclusions.

Notations: Random variables are displayed in sans serif, upright fonts; their realizations in serif, italic fonts. Vectors and matrices are denoted by bold lowercase and uppercase letters, respectively. For example, a random variable and its realization are denoted by x and x; a random vector and its realization are denoted by $\mathbf{x}$ and $\boldsymbol{x}$; a random matrix and its realization are denoted by $\mathbf{X}$ and $\boldsymbol{X}$, respectively. Sets are

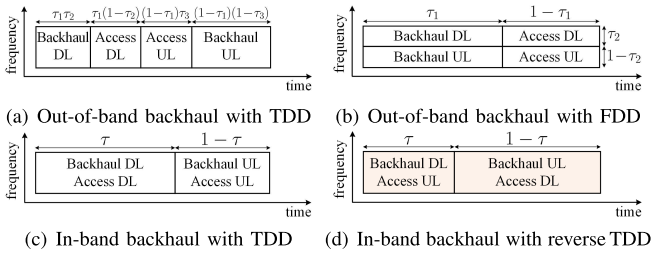

Fig. 1. Different types of wireless backhaul schemes with different duplexing modes. The resource allocation factors $\tau, \tau_1, \tau_2, \tau_3 \in [0, 1]$ can be adjusted to meet various UL-DL traffic demands.

denoted by calligraphic font. For example, a set is denoted by $\mathcal{X}$. The m-by-m identity matrix is denoted by $\boldsymbol{I}_m$: the subscript is removed when the dimension is clear from the context. The transpose and conjugate transpose are denoted by $(\cdot)^{\mathrm{T}}$ and $(\cdot)^{\dagger}$, respectively. The set of complex numbers and its mth Cartesian power are denoted by $\mathbb{C}$ and $\mathbb{C}^m$, respectively. The expectation operator is denoted by $\mathbb{E}\{\cdot\}$.

II. System Model

This section describes the IAB architecture, channel models, and signal models for the proposed TSN.

A. In-Band IAB for TSNs

Consider a TSN with a single GEO satellite providing wireless backhaul links to a terrestrial network within the area of a single satellite beam.[1] The terrestrial network consists of B gNBs and U UEs. The gNBs are equipped with an antenna array of M elements, while each UE has a single antenna. The satellite has a directional antenna with a fixed radiation pattern. The gNBs cooperatively transmit/receive the signals to/from the satellite and UEs by exploiting the multi-node diversity and BF gain. The TSN can use both *Ka*-band and *S*-band for providing potential broadband services in various situations, including an urban hotspot, unexpected disaster, backhaul infrastructure failure, and isolated rural areas. Due to the limited link budget, we assume that the direct links between the GEO satellite and UEs are not considered for broadband services.

In the TSN with IAB, an efficient signaling scheme between access and backhaul links is necessary within limited time/frequency resources. For example, the UL and DL signaling scheme between access and backhaul relies on either the out-of-band backhauling or the in-band backhauling. In the case of the out-of-band backhauling, the access and backhaul use orthogonal time/frequency resources, in which TDD or frequency division duplexing (FDD) can be used for UL and DL signaling as in Fig. 1(a) and Fig. 1(b), respectively. In the case of the in-band backhauling, the same frequency band is shared between the access and backhaul, in which TDD or reverse TDD can be used as in Fig. 1(c) and Fig. 1(d). Since in-band backhauling has been shown to be more efficient than out-of-band backhauling in terms of resource usage [43], [44], this paper considers the in-band operation between the access and backhaul networks with sophisticated interference management for inter-/intra- terrestrial and satellite networks.

[1]Inter-beam interference from satellite beams is not considered by assuming that the beams are assigned with different frequency bands or have a sharp beamwidth using a large antenna aperture. In addition, an interesting future work can be the design of spectrally efficient and robust TSNs for LEO satellite mega-constellations with extremely high mobility to deliver low latency broadband data services anywhere on the Earth. The related works for the mobility of LEO satellites are in [58], [59], and [60].

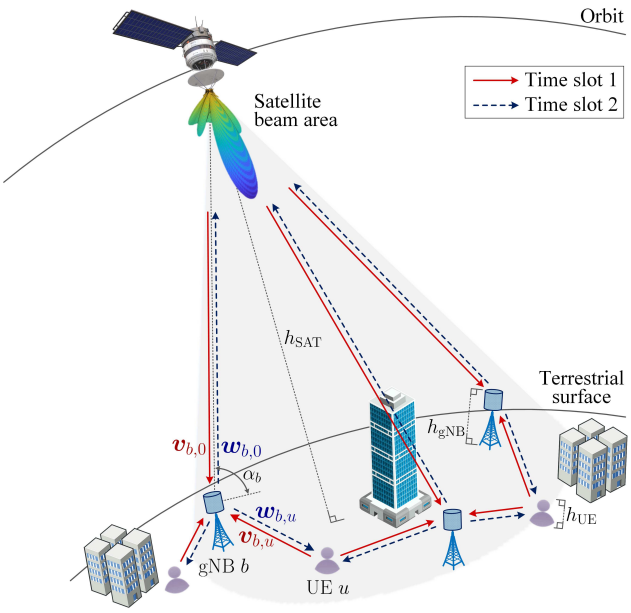

Fig. 2. The proposed TSN with in-band IAB based on reverse TDD and gNB cooperation. The satellite altitude, gNB height, and UE height are denoted by h_{SAT}, h_{gNB}, and h_{UE}, respectively. The elevation angle of the satellite from the bth gNB is denoted by α_b. The transmit and receive BF vectors at the bth gNB are denoted by $\boldsymbol{w}_{b,u}$ and $\boldsymbol{v}_{b,u}$, respectively. This figure shows a single terrestrial network, while multiple terrestrial networks in different regions can use the same satellite beam at different frequency subbands.

B. Reverse TDD for TSNs With IAB

For efficient channel usage, resource allocation is necessary according to UL and DL data traffic demands [61]. In 5G NR, dynamic TDD is considered with various UL-DL configurations for flexible traffic control [62]. Since the TSN with in-band IAB shares the same spectrum between the access and backhaul links, TDD operation needs to be adjusted with time allocation considering the end-to-end performance between the satellite and UEs.

In TSNs with in-band IAB, TDD can be applied to the access and backhaul networks in two different ways, as shown in Fig. 1(c) and Fig. 1(d). In Fig. 1(c), either UL or DL is scheduled for both access and backhaul networks at a given time slot, which may require in-band full duplex operations at gNBs. In this case, the gNBs may suffer from self-interference, while the UEs and satellite may suffer from interference between access and backhaul links. Alternatively, reverse TDD in Fig. 1(d) is useful for interference management between the access and backhaul links [36], [40]. In this scheme, the orders of UL and DL transmissions are reversed over access and backhaul networks, which is illustrated in Fig. 2. At time slot 1, the backhaul DL and access UL signals are simultaneously transmitted from the satellite and UEs to the gNBs. At time slot 2, the backhaul UL and access

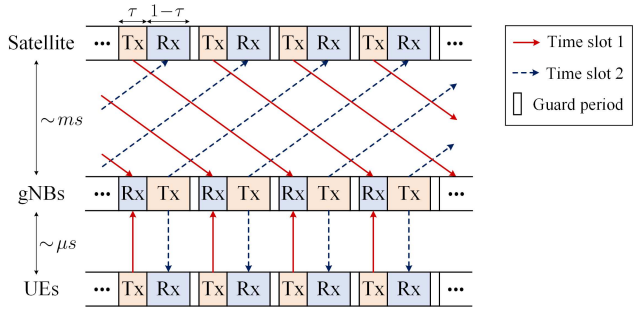

Fig. 3. Illustration of the reverse TDD operation in the TSN with IAB. The TDD frame length is chosen to be a fraction of the propagation delay of the backhaul link. 'Tx' and 'Rx' mean 'transmit' and 'receive', respectively.

DL signals are simultaneously transmitted from the gNBs to the satellite and UEs. By doing so, self-interference can be avoided using half duplex gNBs, and interference between access and backhaul can be mitigated by BF design at the gNBs. In addition, the time fraction τ in Fig. 1(d) can be optimized between time slot 1 and time slot 2 for efficient resource usage.

Reverse TDD is particularly useful in TSNs to overcome a long propagation delay in the non-terrestrial channel. The use of TDD requires a guard period between UL and DL that equals the maximum round trip propagation delay for interference avoidance and timing advance. This is not efficient for satellite communication systems due to long propagation delay, e.g., 119.29 ms from a terrestrial gNB to a GEO satellite at the elevation angle of 90°. Therefore, most satellite communication systems adopt FDD. In the reverse TDD setting, a data frame length can be chosen to be a fraction of the propagation delay so that the UL and DL signals for both access and backhaul links can be transmitted consecutively in separated time slots, as shown in Fig. 3 [63].

C. Non-Terrestrial and Terrestrial Channel Models

The non-terrestrial and terrestrial channels have different propagation characteristics in terms of both large-scale and small-scale gains [64], [65], [66]. In particular, the non-terrestrial channels are affected by the elevation angle α_b. We use a general expression for both the non-terrestrial and terrestrial channels considering reverse TDD. The backhaul DL channel from the satellite to the bth gNB and the access UL channel from the uth UE to the bth gNB are commonly expressed by an $M \times 1$ vector as

$$\mathbf{h}_{b,u} = \xi_{b,u}\boldsymbol{\omega}_{b,u} \tag{1}$$

for $b = 1, 2, \ldots, B$ and $u = 0, 1, \ldots, U$; the index $u = 0$ indicates the satellite while $u \geqslant 1$ indicates the terrestrial UEs. The 3GPP non-terrestrial and terrestrial models are used for both the large-scale channel $\xi_{b,u}$ and the small-scale channel $\boldsymbol{\omega}_{b,u}$ according to [65] and [66]. Assuming the channel reciprocity in TDD operations, the channel vectors for the backhaul UL and access DL are denoted by $\mathbf{h}_{b,u}^{\dagger}$.

1) Probabilistic line-of-sight (LOS): Both the large-scale and small-scale channels in (1) depend on the existence of the LOS path, which is randomly determined as the Bernoulli random variable $\mathsf{X}_{b,u} \in \{0, 1\}$ with respect to the LOS probability function $P_{\mathrm{LOS}}(\cdot)$ [65], [66], [67]. For non-terrestrial channels, the LOS probability is represented by $P_{\mathrm{LOS}}(e, \alpha_b)$, which depends on the terrestrial environment $e \in \{\text{dense urban, urban, suburban, and rural}\}$ and the elevation angle α_b between the satellite and the bth gNB [65, Table 6.6.1-1]. For terrestrial channels, it is represented by $P_{\mathrm{LOS}}(e, d_{b,u}, h_{\mathrm{gNB}}, h_{\mathrm{UE}})$, where $e \in \{\mathrm{RMa}, \mathrm{UMi}, \mathrm{UMa}, \mathrm{Indoor}, \mathrm{InF}, \text{and } \mathrm{InH}\}$; $d_{b,u}$ is the distance between the bth gNB and the uth UE; h_{gNB} and h_{UE} are the antenna heights [66, Table 7.4.2-1].

2) Large-Scale Channel: The large-scale channel gain in (1) is expressed by [65] and [66] as

$$\xi_{b,u} = \sqrt{\frac{G_{b,u}^{\mathrm{TX}} G_{b,u}^{\mathrm{RX}}}{\mathsf{L}_{b,u}}}$$

with

$$\mathsf{L}_{b,u} = \begin{cases} A_{b,0}^{\mathrm{FS}}\, \mathsf{A}_{b,0}^{\mathrm{SF}}\, \mathsf{A}_{b,0}^{\mathrm{CL}}\, A_{b,0}^{\mathrm{G}}\, A_{b,0}^{\mathrm{S}} & \text{for } u = 0 \\ A_{b,u}^{\mathrm{FS}}\, \mathsf{A}_{b,u}^{\mathrm{SF}} & \text{for } u = 1, 2, \ldots, U \end{cases}$$

where $G_{b,u}^{\mathrm{TX}}$ and $G_{b,u}^{\mathrm{RX}}$ denote the antenna gains at transmitter and receiver, respectively. For the satellite, $G_{b,0}^{\mathrm{TX}}$ in DL and $G_{b,0}^{\mathrm{RX}}$ in UL are determined by the beam pattern of the antenna aperture as a function of α_b. For the gNBs and UEs, omnidirectional antenna elements with unit gain are assumed. The loss $\mathsf{L}_{b,u}$ consists of different attenuation terms, which depend on $\mathsf{X}_{b,u}$, α_b, $d_{b,u}$, and the frequency f_{c}. To be specific, the free space pathloss, $A_{b,u}^{\mathrm{FS}}$, depends on f_{c} and $d_{b,u}$. The shadow fading loss $\mathsf{A}_{b,u}^{\mathrm{SF}}$ follows the log-normal distribution such that $\ln \mathsf{A}_{b,0}^{\mathrm{SF}} \sim \mathcal{N}\big(0, \sigma_{\mathrm{SF}}^2(f_{\mathrm{c}}, \mathsf{X}_{b,0}, \alpha_b)\big)$ and $\ln \mathsf{A}_{b,u}^{\mathrm{SF}} \sim \mathcal{N}\big(0, \sigma_{\mathrm{SF}}^2(f_{\mathrm{c}}, \mathsf{X}_{b,u})\big)$ for $u \geqslant 1$. The clutter loss $\mathsf{A}_{b,0}^{\mathrm{CL}}$ depends on f_{c}, $\mathsf{X}_{b,0}$, and α_b. The loss $A_{b,0}^{\mathrm{G}}$ is the attenuation due to atmospheric gasses, which is given by $A_{b,0}^{\mathrm{G}} = A_{\mathrm{z}}(f_{\mathrm{c}})/\sin(\alpha_b)$ under a clear sky, where $A_{\mathrm{z}}(f_{\mathrm{c}})$ is the zenith attenuation as a function of f_{c} [65]. The loss $A_{b,0}^{\mathrm{S}}$ is the attenuation due to either ionospheric scintillation (for below 6 GHz) or tropospheric scintillation (for above 6 GHz). The building entry loss is ignored, considering the outdoor scenarios. The behaviors of the 3GPP non-terrestrial channels for different α_b are shown in Fig. 4.

3) Small-Scale Channel: The small-scale channel vector in (1) can be expressed by [65] and [66] as

$$\boldsymbol{\omega}_{b,u} = \begin{cases} \boldsymbol{\omega}_{b,u}^{(\mathrm{L})} & \text{if } \chi_{b,u} = 1 \\ \boldsymbol{\omega}_{b,u}^{(\mathrm{N})} & \text{if } \chi_{b,u} = 0 \end{cases}$$

with

$$\boldsymbol{\omega}_{b,u}^{(\mathrm{L})} \triangleq \sqrt{\frac{\kappa_{b,u}}{\kappa_{b,u}+1}}\boldsymbol{a}\big(\phi_{b,u}, \theta_{b,u}\big) + \sqrt{\frac{1}{\kappa_{b,u}+1}} \sum_{k=1}^{K_{b,u}} \sum_{n=1}^{N_{b,u}} \sqrt{\frac{\varrho_{b,u}^{(k)}}{N_{b,u}}}\beta_{b,u}^{(k,n)}\boldsymbol{a}\big(\varphi_{b,u}^{(k,n)}, \vartheta_{b,u}^{(k,n)}\big)$$

$$\boldsymbol{\omega}_{b,u}^{(\mathrm{N})} \triangleq \sum_{k=1}^{K_{b,u}} \sum_{n=1}^{N_{b,u}} \sqrt{\frac{\varrho_{b,u}^{(k)}}{N_{b,u}}}\beta_{b,u}^{(k,n)}\boldsymbol{a}\big(\varphi_{b,u}^{(k,n)}, \vartheta_{b,u}^{(k,n)}\big)$$

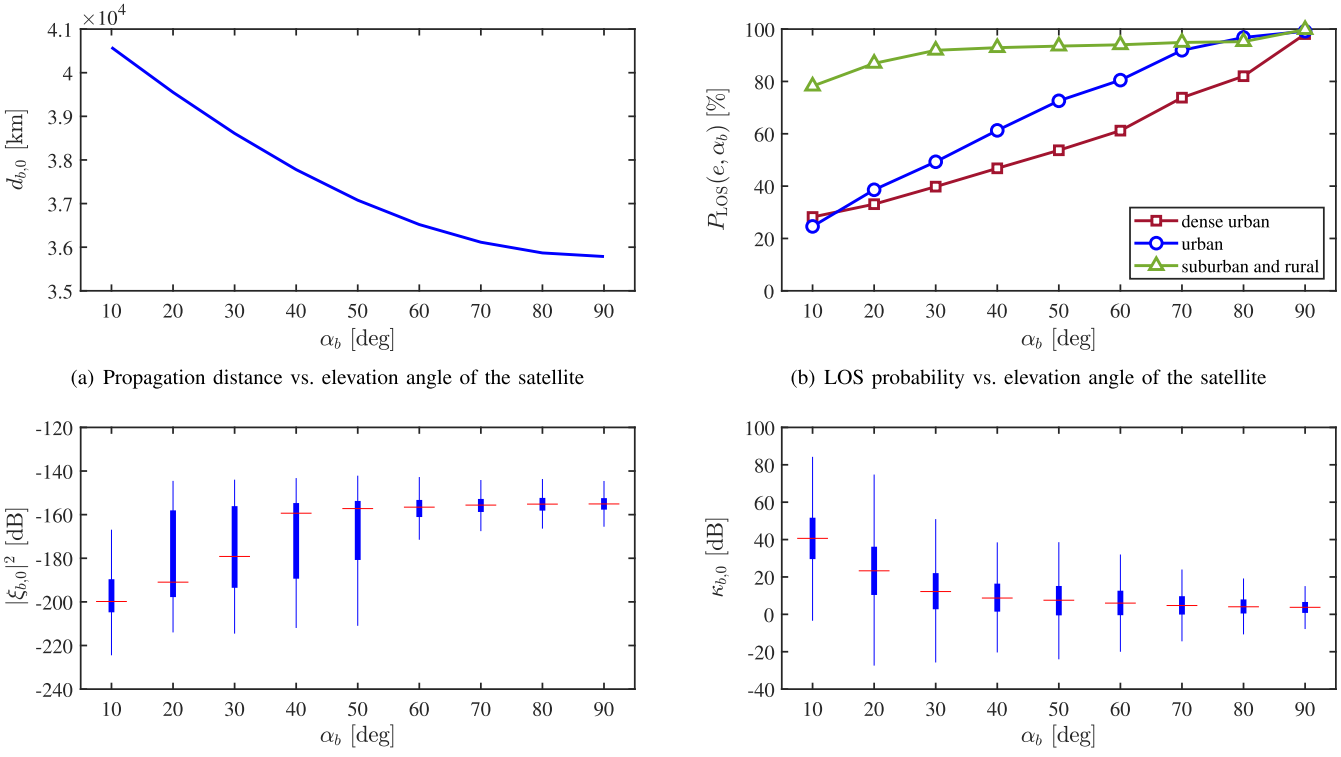

(a) Propagation distance vs. elevation angle of the satellite

(b) LOS probability vs. elevation angle of the satellite

(c) Large-scale channel gain vs. elevation angle of the satellite

(d) Rician K-factor vs. elevation angle of the satellite

Fig. 4. Non-terrestrial channel characteristics between a GEO satellite and a gNB with $h_{\mathrm{SAT}} = 35,786$ km and $h_{\mathrm{gNB}} = 10$ m. In (c) and (d), the 3GPP urban scenario is assumed with $f_{\mathrm{c}} = 30$ GHz. A red horizontal line indicates the median of the random variables, and the bottom and top edges of the blue boxes indicate the 25th and 75th percentiles, respectively.

where $\boldsymbol{\omega}_{b,u}^{(\mathrm{L})}$ is the Rician channel model including the LOS path and the clustered non-line-of-sight (NLOS) paths, while $\boldsymbol{\omega}_{b,u}^{(\mathrm{N})}$ includes only NLOS paths. The Rician K-factor is denoted by the random variable $\kappa_{b,u}$, which is given in [65] and [66] according to the environment and α_b. For given $\chi_{b,u}$, the NLOS paths form $K_{b,u}$ scattering clusters each with $N_{b,u}$ rays, where the kth cluster has the normalized power $\varrho_{b,u}^{(k)}$ satisfying $\sum_k \varrho_{b,u}^{(k)} = 1$ [66]. The complex path gain is denoted by $\beta_{b,u}^{(k,n)}$. The array response vector of the gNB is denoted by $\boldsymbol{a}(\cdot)$, for which the mth element is given by $[\boldsymbol{a}(\phi,\theta)]_m \triangleq 1/\sqrt{M}\exp\{-j\boldsymbol{q}_m^{\mathrm{T}}\boldsymbol{k}(\phi,\theta)\}$, $m = 1, 2, \ldots, M$. The vector $\boldsymbol{q}_m$ is the relative position vector of the mth antenna element with the origin at the center of the array. $\boldsymbol{k}(\phi,\theta) \triangleq \bar{k}[\cos\phi\sin\theta, \sin\phi\sin\theta, \cos\theta]^{\mathrm{T}}$ is the wave vector, where $\bar{k}$ is the wave number. The azimuth and zenith angles are denoted by $\phi_{b,u}$ and $\theta_{b,u}$ for the LOS path, respectively, and by $\varphi_{b,u}^{(n,m)}$ and $\vartheta_{b,u}^{(n,m)}$ for the random NLOS paths, respectively.

D. Signal Model

The gNBs are assumed to obtain the channel state information using pilot signals transmitted from the satellite and UEs at time slot 1. This information is shared among the gNBs and used for cooperative data transmission in both time slot 1 and time slot 2 based on the channel reciprocity. Since the relative positions of the GEO satellite and gNBs are fixed, the channel coherence time of the satellite backhaul link is assumed to be larger than the round-trip propagation time. This is a benefit of the GEO satellite-based backhauling compared to non-GEO satellite-based networks or direct access networks between the satellite and UEs.

At time slot 1, the satellite and UEs transmit the backhaul DL signal and access UL signals to the gNBs. For given channels, the received signal $\tilde{\mathbf{y}}_b' \in \mathbb{C}^M$ at the bth gNB is expressed by

$$\tilde{\mathbf{y}}_b' = \sqrt{P_0'}\boldsymbol{h}_{b,0}\mathsf{x}_0' + \sum_{u=1}^{U}\sqrt{P_u'}\boldsymbol{h}_{b,u}\mathsf{x}_u' + \mathbf{n}_b' \tag{2}$$

where P_u' is the transmit power of the satellite and the uth UE when $u = 0$ and $u \geqslant 1$, respectively. The transmitted data symbols from the satellite and UEs are denoted by independent random variables x_0' and x_u' for $u \geqslant 1$, respectively, which satisfy $\mathbb{E}\{|\mathsf{x}_u'|^2\} = 1$. The additive noise at the bth gNB is denoted by $\mathbf{n}_b'$, which follows the circularly-symmetric complex Gaussian distribution, i.e., $\mathbf{n}_b' \sim \mathcal{CN}(\mathbf{0}, (\sigma')^2\boldsymbol{I}_M)$, where $(\sigma')^2$ is the average noise power at the gNB. Exploiting gNB cooperation and multi-antenna processing gain [68], [69], [70], [71], [72], the signals $\tilde{\mathbf{y}}_b' \forall b$ in (2) are combined with the BF vectors $\boldsymbol{v}_{b,u} \in \mathbb{C}^M \forall b$ to detect the transmitted symbol for $u = 0, 1, \ldots, U$ as follows,

$$\begin{aligned}\mathsf{y}_u' &= \sum_{b=1}^{B}\boldsymbol{v}_{b,u}^{\dagger}\tilde{\mathbf{y}}_b' \\ &= \sum_{b=1}^{B}\sqrt{P_0'}\boldsymbol{v}_{b,u}^{\dagger}\boldsymbol{h}_{b,0}\mathsf{x}_0' + \sum_{b=1}^{B}\sum_{j=1}^{U}\sqrt{P_j'}\boldsymbol{v}_{b,u}^{\dagger}\boldsymbol{h}_{b,j}\mathsf{x}_j' + \sum_{b=1}^{B}\boldsymbol{v}_{b,u}^{\dagger}\mathbf{n}_b'.\end{aligned} \tag{3}$$

At time slot 2, the gNBs simultaneously transmit the backhaul UL signal and access DL signals to the satellite and UEs, respectively. The received signals at the satellite and the uth UE are expressed by

$$\mathsf{y}_0 = \sum_{b=1}^{B} \sqrt{P_{b,0}} \boldsymbol{h}_{b,0}^{\dagger} \boldsymbol{w}_{b,0} \mathsf{x}_0 + \sum_{b=1}^{B} \sum_{j=1}^{U} \sqrt{P_{b,j}} \boldsymbol{h}_{b,0}^{\dagger} \boldsymbol{w}_{b,j} \mathsf{x}_j + \mathsf{n}_0 \tag{4}$$

and

$$\mathsf{y}_u = \sum_{b=1}^{B} \sqrt{P_{b,u}} \boldsymbol{h}_{b,u}^{\dagger} \boldsymbol{w}_{b,u} \mathsf{x}_u + \sum_{b=1}^{B} \sum_{\substack{j=0,\\ j\neq u}}^{U} \sqrt{P_{b,j}} \boldsymbol{h}_{b,u}^{\dagger} \boldsymbol{w}_{b,j} \mathsf{x}_j + \mathsf{n}_u \tag{5}$$

for $u = 1, 2, \ldots U$, respectively. The transmit power scalings at the bth gNB for the satellite and the uth UE are denoted by $P_{b,0}$ and $P_{b,u}$ for $u \geqslant 1$, respectively. Similarly, the transmit BF vectors used at the bth gNB are denoted by $\boldsymbol{w}_{b,u} \in \mathbb{C}^M$. The transmitted symbol from the gNBs to the satellite or the uth UE is denoted by x_u, which satisfies $\mathbb{E}\{|\mathsf{x}_u|^2\} = 1$. The total transmit power at each gNB is limited by P_{t} such that $\sum_{u=0}^{U} \|\boldsymbol{w}_{b,u}\|^2 P_{b,u} \leqslant P_{\mathrm{t}}$. The noise is distributed as $\mathsf{n}_u \sim \mathcal{CN}(0, \sigma_u^2)$, where σ_u^2 is the average noise power at the satellite or the uth UE.

E. End-to-End Achievable Sum Rate

From (3), the signal-to-interference-plus-noise ratios (SINRs) for the backhaul DL and access UL signals at the gNBs can be expressed for given channels by

$$\gamma_0^{\mathrm{DL}} = \frac{\left|\sum_{b=1}^{B} \sqrt{P_0'} \boldsymbol{v}_{b,0}^{\dagger} \boldsymbol{h}_{b,0}\right|^2}{\sum_{j=1}^{U} \left|\sum_{b=1}^{B} \sqrt{P_j'} \boldsymbol{v}_{b,0}^{\dagger} \boldsymbol{h}_{b,j}\right|^2 + (\sigma')^2 \sum_{b=1}^{B} \left\|\boldsymbol{v}_{b,0}\right\|^2} \tag{6a}$$

and

$$\gamma_u^{\mathrm{UL}} = \frac{\left|\sum_{b=1}^{B} \sqrt{P_u'} \boldsymbol{v}_{b,u}^{\dagger} \boldsymbol{h}_{b,u}\right|^2}{\sum_{\substack{j=0,\\ j\neq u}}^{U} \left|\sum_{b=1}^{B} \sqrt{P_j'} \boldsymbol{v}_{b,u}^{\dagger} \boldsymbol{h}_{b,j}\right|^2 + (\sigma')^2 \sum_{b=1}^{B} \left\|\boldsymbol{v}_{b,u}\right\|^2} \tag{6b}$$

for $u = 1, 2, \ldots, U$, respectively.

From (4) and (5), the SINRs for the backhaul UL at the satellite and the access DL at the uth UE can be expressed for given channels by

$$\gamma_0^{\mathrm{UL}} = \frac{\left|\sum_{b=1}^{B} \sqrt{P_{b,0}} \boldsymbol{h}_{b,0}^{\dagger} \boldsymbol{w}_{b,0}\right|^2}{\sum_{j=1}^{U} \left|\sum_{b=1}^{B} \sqrt{P_{b,j}} \boldsymbol{h}_{b,0}^{\dagger} \boldsymbol{w}_{b,j}\right|^2 + \sigma_0^2} \tag{7a}$$

and

$$\gamma_u^{\mathrm{DL}} = \frac{\left|\sum_{b=1}^{B} \sqrt{P_{b,u}} \boldsymbol{h}_{b,u}^{\dagger} \boldsymbol{w}_{b,u}\right|^2}{\sum_{j=0, j\neq u}^{U} \left|\sum_{b=1}^{B} \sqrt{P_{b,j}} \boldsymbol{h}_{b,u}^{\dagger} \boldsymbol{w}_{b,j}\right|^2 + \sigma_u^2} \tag{7b}$$

for $u = 1, 2, \ldots, U$, respectively.

In the TSN with IAB, the end-to-end achievable sum rate of the UL or DL is limited by the minimum of the access and backhaul networks. From (6) and (7), the end-to-end achievable sum rates per unit bandwidth for UL and DL can be expressed using the time fraction τ of the reverse TDD as [73], [74], and [43]

$$R^{\mathrm{UL}} = \min\left\{\tau \sum_{u=1}^{U} \log_2\left(1 + \gamma_u^{\mathrm{UL}}\right),\ (1-\tau) \log_2\left(1 + \gamma_0^{\mathrm{UL}}\right)\right\} \tag{8a}$$

$$R^{\mathrm{DL}} = \min\left\{\tau \log_2\left(1 + \gamma_0^{\mathrm{DL}}\right),\ (1-\tau) \sum_{u=1}^{U} \log_2\left(1 + \gamma_u^{\mathrm{DL}}\right)\right\}. \tag{8b}$$

III. Problem Formulation for UL-DL Rate Region Maximization

To maximize the UL-DL rate region of the TSN with IAB, the receive BF, transmit BF, and power allocation at the gNBs are jointly optimized with time allocation for every channel coherence time. For fixed transmit powers of the satellite and UEs, i.e., $P_u' \forall u$, the receive BF $\boldsymbol{v}_{b,u} \forall b, u$ can be optimized first. Then a joint design problem for the transmit BF, power allocation, and time allocation is formulated to optimize $\boldsymbol{w}_{b,u}$, $P_{b,u} \forall b, u$, and τ.

A. Receive BF at gNBs

For given $P_u' \forall u$, the SINRs in (6) can be expressed by tractable forms by defining the following two concatenated vectors

$$\boldsymbol{h}_u \triangleq \left[\boldsymbol{h}_{1,u}^{\mathrm{T}}, \boldsymbol{h}_{2,u}^{\mathrm{T}}, \ldots, \boldsymbol{h}_{B,u}^{\mathrm{T}}\right]^{\mathrm{T}} \tag{9a}$$

$$\boldsymbol{v}_u \triangleq \left[\boldsymbol{v}_{1,u}^{\mathrm{T}}, \boldsymbol{v}_{2,u}^{\mathrm{T}}, \ldots, \boldsymbol{v}_{B,u}^{\mathrm{T}}\right]^{\mathrm{T}} \tag{9b}$$

for $u = 0, 1, \ldots, U$. Using (9), γ_0^{DL} and γ_u^{UL} in (6a) and (6b) can be expressed by functions of $\boldsymbol{v}_u$ as

$$\gamma_0^{\mathrm{DL}}(\boldsymbol{v}_0) = \frac{P_0' \boldsymbol{v}_0^{\dagger} \left(\boldsymbol{h}_0 \boldsymbol{h}_0^{\dagger}\right) \boldsymbol{v}_0}{\boldsymbol{v}_0^{\dagger} \left(\sum_{j=1}^{U} P_j' \boldsymbol{h}_j \boldsymbol{h}_j^{\dagger} + (\sigma')^2 \boldsymbol{I}\right) \boldsymbol{v}_0} \tag{10a}$$

and

$$\gamma_u^{\mathrm{UL}}(\boldsymbol{v}_u) = \frac{P_u' \boldsymbol{v}_u^{\dagger} \left(\boldsymbol{h}_u \boldsymbol{h}_u^{\dagger}\right) \boldsymbol{v}_u}{\boldsymbol{v}_u^{\dagger} \left(\sum_{j=0, j\neq u}^{U} P_j' \boldsymbol{h}_j \boldsymbol{h}_j^{\dagger} + (\sigma')^2 \boldsymbol{I}\right) \boldsymbol{v}_u} \tag{10b}$$

respectively.

From (10), each vector $\boldsymbol{v}_u \in \mathbb{C}^{BM}$ can be optimized to maximize the corresponding SINR at time slot 1 by solving the following problem,

$$\boldsymbol{v}_u^* = \underset{\boldsymbol{v}_u}{\operatorname{argmax}} \frac{P_u' \boldsymbol{v}_u^{\dagger} \left(\boldsymbol{h}_u \boldsymbol{h}_u^{\dagger}\right) \boldsymbol{v}_u}{\boldsymbol{v}_u^{\dagger} \left(\sum_{j=0, j\neq u}^{U} P_j' \boldsymbol{h}_j \boldsymbol{h}_j^{\dagger} + (\sigma')^2 \boldsymbol{I}_{BM}\right) \boldsymbol{v}_u} \tag{11}$$

which is known as the generalized Rayleigh quotient problem [75]. The solution to the problem in (11) can be obtained by the generalized eigenvector having the largest eigenvalue between the matrices $P_u' \boldsymbol{h}_u \boldsymbol{h}_u^{\dagger}$ and $\sum_{j=0, j\neq u}^{U} P_j' \boldsymbol{h}_j \boldsymbol{h}_j^{\dagger} + (\sigma')^2 \boldsymbol{I}_{BM}$.

B. Joint Optimization Problem of Transmit BF, Power Allocation, and Time Allocation

Using $\boldsymbol{v}_u^* \forall u$ in (11), the achievable rates per unit bandwidth of the access UL and backhaul DL are fixed by

$$\tilde{R}^{\mathrm{UL}} \triangleq \sum_{u=1}^{U} \log_2\left(1+\gamma_u^{\mathrm{UL}}(\boldsymbol{v}_u^*)\right) \tag{12a}$$

$$\tilde{R}^{\mathrm{DL}} \triangleq \log_2\left(1+\gamma_0^{\mathrm{DL}}(\boldsymbol{v}_0^*)\right). \tag{12b}$$

Substituting (12a) and (12b) into (8a) and (8b), respectively, $\boldsymbol{w}_{b,u}$, $P_{b,u} \forall b, u$, and τ are jointly optimized to maximize the UL-DL rate region of the TSN. To formulate the optimization problem, the design variable set and the power constraint are defined by

$$\mathcal{S} \triangleq \left\{\boldsymbol{w}_{b,u}, P_{b,u} : b = 1, 2, \ldots, B, u = 0, 1, \ldots, U\right\} \tag{13}$$

$$\check{\mathcal{S}}_0 \triangleq \left\{\mathcal{S} : \sum_{u=0}^{U} \|\boldsymbol{w}_{b,u}\|^2 P_{b,u} \leqslant P_{\mathrm{t}} \text{ and } P_{b,u} \geqslant 0 \forall b\right\}. \tag{14}$$

Using (13), the SINRs in (7a) and (7b) can be expressed as functions of $\mathcal{S}$ such that $\gamma_0^{\mathrm{UL}}(\mathcal{S})$ and $\gamma_u^{\mathrm{DL}}(\mathcal{S})$. Then we aim to maximize the weighted sum rates per unit bandwidth of the UL and DL, which is defined by using (8) and (12) as

$$f(\mathcal{S}, \tau) \triangleq \zeta \min\left\{\tau \tilde{R}^{\mathrm{UL}}, (1-\tau)\log_2\left(1+\gamma_0^{\mathrm{UL}}(\mathcal{S})\right)\right\} + (1-\zeta)\min\left\{\tau \tilde{R}^{\mathrm{DL}}, (1-\tau)\sum_{u=1}^{U}\log_2\left(1+\gamma_u^{\mathrm{DL}}(\mathcal{S})\right)\right\} \tag{15}$$

where ζ is a known weight for controlling the trade-off between the UL and DL rates. From (13), (14), and (15), the optimization problem is formulated as

$$\mathscr{P}_0 : \underset{\mathcal{S}\subseteq\check{\mathcal{S}}_0,\, 0<\tau<1}{\text{maximize}} \quad f(\mathcal{S}, \tau).$$

By solving $\mathscr{P}_0$ for different values of ζ, an UL-DL rate region can be obtained. As an extreme example, if there is a traffic demand for DL but not for UL, ζ can be set to zero.

C. Optimization Strategy

The common power level p_u for the uth UE or satellite commonly used at all the gNBs is introduced for designing an efficient algorithm. Without loss of generality, using the variable p_u, the feasible constraint set $\check{\mathcal{S}}_0$ in the problem $\mathscr{P}_0$ can be equivalently expressed by $\check{\mathcal{S}}_1$ as [76]

$$\check{\mathcal{S}}_1 \triangleq \left\{\mathcal{S} : \|\boldsymbol{w}_u\|^2 = 1 \forall u, \sum_{u=0}^{U}\|\boldsymbol{w}_{b,u}\|^2 p_u \leqslant P_{\mathrm{t}} \text{ and } P_{b,u} = p_u \geqslant 0 \forall b\right\} \tag{16}$$

where $\boldsymbol{w}_u \triangleq \left[\boldsymbol{w}_{1,u}^{\mathrm{T}}, \boldsymbol{w}_{2,u}^{\mathrm{T}}, \ldots, \boldsymbol{w}_{B,u}^{\mathrm{T}}\right]^{\mathrm{T}} \in \mathbb{C}^{BM}$. Note that power control among the gNBs is still possible by the concatenated vector $\boldsymbol{w}_u$ even if the common power level is used.

After substituting $\check{\mathcal{S}}_0$ with $\check{\mathcal{S}}_1$, the problem $\mathscr{P}_0$ is expressed by a bilevel optimization formulation containing a lower-level problem nested within an upper-level problem as follows [77],

$$\mathscr{P}_0 : \underset{0<\tau<1}{\text{maximize}} \quad f^*(\tau) \tag{17}$$

where $f^*(\tau)$ corresponds to the optimal solution to the lower-level problem, defined by a function of τ as

$$\mathscr{P}_1(\tau) : \underset{\mathcal{S}\subseteq\check{\mathcal{S}}_1}{\text{maximize}} \quad f(\mathcal{S}, \tau).$$

Since the end-to-end UL and DL rates in the first and second terms of (15) may be limited by $\tau\tilde{R}^{\mathrm{UL}}$ and $\tau\tilde{R}^{\mathrm{DL}}$, respectively, $\mathcal{S}$ should be designed such that the transmit power is not excessively allocated to one of the backhaul UL or the access DL in solving $\mathscr{P}_1(\tau)$. For example, if $(1-\tau)\log_2\left(1+\gamma_0^{\mathrm{UL}}(\mathcal{S})\right) > \tau\tilde{R}^{\mathrm{UL}}$ and $(1-\tau)\sum_{u=1}^{U}\log_2\left(1+\gamma_u^{\mathrm{DL}}(\mathcal{S})\right) < \tau\tilde{R}^{\mathrm{DL}}$, the variable $\mathcal{S}$ can be adjusted to reduce $\log_2\left(1+\gamma_0^{\mathrm{UL}}(\mathcal{S})\right)$ and increase $\sum_{u=1}^{U}\log_2\left(1+\gamma_u^{\mathrm{DL}}(\mathcal{S})\right)$ for a higher value of $f(\mathcal{S}, \tau)$. In this way, the power usage of the gNBs needs to be balanced between the backhaul UL and the access DL to maximize the objective value.

Our strategy is to firstly obtain an initial solution assuming no bottleneck in end-to-end links, i.e., $\tilde{R}^{\mathrm{UL}} = \infty$ and $\tilde{R}^{\mathrm{DL}} = \infty$ in $\mathscr{P}_1(\tau)$ regardless of the value of τ. Then further optimization process will be conducted considering the bottleneck. The initial problem can be seen as the conventional weighted sum rate (WSR) maximization problem such that

$$\mathring{\mathscr{P}}_1 : \underset{\mathcal{S}\subseteq\check{\mathcal{S}}_1}{\text{maximize}} \quad \mathring{f}(\mathcal{S})$$

where $\mathring{f}(\mathcal{S}) = \zeta\log_2\left(1+\gamma_0^{\mathrm{UL}}(\mathcal{S})\right) + (1-\zeta)\sum_{u=1}^{U}\log_2\left(1+\gamma_u^{\mathrm{DL}}(\mathcal{S})\right)$. The problem $\mathring{\mathscr{P}}_1$ can be solved by using the existing algorithm in [76]. Once the initial solution is obtained as $\mathring{\mathcal{S}}$ from $\mathring{\mathscr{P}}_1$, the problem $\mathscr{P}_1(\tau)$ can be modified to a constrained maximization problem depending on the values of $\mathring{\mathcal{S}}$ and τ. Specifically, substituting $\mathring{\mathcal{S}}$ into $f(\mathcal{S}, \tau)$ can give four different cases of formulating a constrained problem, namely, Case A, Case B, Case C, and Case D, according to the determination of the two minimum functions in (15). In particular, we will see that only Case A and Case B need to be considered rather than all the four cases due to the similar structure between $\mathscr{P}_1$ and $\mathring{\mathscr{P}}_1$.

- Case A represents the condition $\tau \in \mathcal{T}_{\mathrm{A}}(\mathring{\mathcal{S}})$ meaning that both R^{UL} and R^{DL} are limited by the access links, where the set $\mathcal{T}_{\mathrm{A}}(\mathring{\mathcal{S}})$ is defined by

$$\mathcal{T}_{\mathrm{A}}(\mathring{\mathcal{S}}) \triangleq \left\{\tau : (1-\tau)\log_2\left(1+\gamma_0^{\mathrm{UL}}(\mathring{\mathcal{S}})\right) \geqslant \tau\tilde{R}^{\mathrm{UL}} \text{ and } (1-\tau)\sum_{u=1}^{U}\log_2\left(1+\gamma_u^{\mathrm{DL}}(\mathring{\mathcal{S}})\right) < \tau\tilde{R}^{\mathrm{DL}}\right\}.$$

  In this case, R^{DL} in (8b) can be improved from the initial optimization result while keeping the same R^{UL} in (8a) by solving the following constrained problem,

$$\mathscr{P}_{1,\mathrm{A}}(\tau) : \underset{\mathcal{S}\subseteq\check{\mathcal{S}}_1}{\text{maximize}} \sum_{u=1}^{U}\log_2\left(1+\gamma_u^{\mathrm{DL}}(\mathcal{S})\right) \quad \text{subject to } \log_2\left(1+\gamma_0^{\mathrm{UL}}(\mathcal{S})\right) \geqslant \frac{\tau}{1-\tau}\tilde{R}^{\mathrm{UL}}.$$

- Case B represents the condition $\tau \in \mathcal{T}_{\mathrm{B}}(\mathring{\mathcal{S}})$ meaning that both R^{UL} and R^{DL} are limited by the backhaul links, where the set $\mathcal{T}_{\mathrm{B}}(\mathring{\mathcal{S}})$ is defined by

$$\mathcal{T}_{\mathrm{B}}(\mathring{\mathcal{S}}) \triangleq \Big\{\tau : (1-\tau)\log_2\big(1+\gamma_0^{\mathrm{UL}}(\mathring{\mathcal{S}})\big) < \tau\tilde{R}^{\mathrm{UL}} \text{ and } (1-\tau)\sum_{u=1}^{U}\log_2\big(1+\gamma_u^{\mathrm{DL}}(\mathring{\mathcal{S}})\big) \geqslant \tau\tilde{R}^{\mathrm{DL}}\Big\}.$$

  In this case, R^{UL} in (8a) can be improved while keeping the same R^{DL} (8b) by solving the following constrained problem,

$$\mathscr{P}_{1,\mathrm{B}}(\tau): \underset{\mathcal{S}\subseteq\mathring{\mathcal{S}}_1}{\text{maximize}} \log_2\big(1+\gamma_0^{\mathrm{UL}}(\mathcal{S})\big) \text{ subject to } \sum_{u=1}^{U}\log_2\big(1+\gamma_u^{\mathrm{DL}}(\mathcal{S})\big) \geqslant \frac{\tau}{1-\tau}\tilde{R}^{\mathrm{DL}}.$$

- The other two cases, i.e., Case C and Case D, do not need further optimization processes because $\mathring{\mathcal{S}}$ is already an optimal solution for the following reasons. For Case C, i.e., when $(1-\tau)\log_2\big(1+\gamma_0^{\mathrm{UL}}(\mathring{\mathcal{S}})\big) \geqslant \tau\tilde{R}^{\mathrm{UL}}$ and $(1-\tau)\sum_{u=1}^{U}\log_2\big(1+\gamma_u^{\mathrm{DL}}(\mathring{\mathcal{S}})\big) \geqslant \tau\tilde{R}^{\mathrm{DL}}$, the objective value of $\mathscr{P}_1(\tau)$ using $\mathring{\mathcal{S}}$ is determined as $\zeta\tau\tilde{R}^{\mathrm{UL}} + (1-\zeta)\tau\tilde{R}^{\mathrm{DL}}$, which cannot be improved anymore. For Case D, i.e., when $(1-\tau)\log_2\big(1+\gamma_0^{\mathrm{UL}}(\mathring{\mathcal{S}})\big) < \tau\tilde{R}^{\mathrm{UL}}$ and $(1-\tau)\sum_{u=1}^{U}\log_2\big(1+\gamma_u^{\mathrm{DL}}(\mathring{\mathcal{S}})\big) < \tau\tilde{R}^{\mathrm{DL}}$, $\mathscr{P}_1(\tau)$ becomes equivalent to $\mathring{\mathscr{P}}_1$.

In summary, the problem $\mathscr{P}_1(\tau)$ can be solved by using $\mathring{\mathscr{P}}_1$, $\mathscr{P}_{1,\mathrm{A}}(\tau)$, and $\mathscr{P}_{1,\mathrm{B}}(\tau)$.

IV. Algorithm Design

In this section, the algorithms to solve the optimization problem $\mathscr{P}_0$ are designed. We first present the outer algorithm according to the strategy in Sec. III. Then the algorithms to solve the problems $\mathscr{P}_{1,\mathrm{A}}(\tau)$ and $\mathscr{P}_{1,\mathrm{B}}(\tau)$ are designed.

A. Outer Algorithm for Problem $\mathscr{P}_0$

The main loop of the outer algorithm is to find an optimal τ, which maximizes $f^*(\tau)$ in (17), where $f^*(\tau)$ corresponds to the solution $\mathcal{S}_\tau^*$ to the lower-level problem $\mathscr{P}_1(\tau)$. According to the strategy explained in Sec. III-C, the lower-level problem $\mathscr{P}_1(\tau)$ is solved for given τ and the initial solution $\mathring{\mathcal{S}}$ obtained by solving $\mathring{\mathscr{P}}_1$. Since the objective function of $\mathscr{P}_0$ has a non-monotonic behavior with respect to τ (which will be presented in Fig. 8), we use the ternary search algorithm to find a local extremum, which is an interval-based divide-and-conquer algorithm generalized from the binary search algorithm [78]. The proposed outer algorithm is summarized in Algorithm 1 where the key steps are explained in the following. In line 3, the lower and upper bounds for searching the optimal value of τ are initialized. In lines 4–30, an optimal τ^* is found via the ternary search algorithm by reducing the search range between $\check{\tau}$ and $\hat{\tau}$. In lines 5 and 6, a third of the interval $[\hat{\tau}, \check{\tau}]$ from the lower and upper bounds are saved as τ_{l} and τ_{r}. In lines 7–24, the objective values are evaluated for both τ_{l} and τ_{r}, and one of them will be chosen to update the optimal τ^*. In lines 9–12, if $\tau \in \mathcal{T}_{\mathrm{A}}(\mathring{\mathcal{S}})$, the problem $\mathscr{P}_{1,\mathrm{A}}(\tau)$ is solved by using Algorithm 2 and Algorithm 3. In lines 15–18, if $\tau \in \mathcal{T}_{\mathrm{B}}(\mathring{\mathcal{S}})$, the problem $\mathscr{P}_{1,\mathrm{B}}(\tau)$ is solved by using Algorithm 4 and Algorithm 5. In lines 25–29, τ_{l} and τ_{r} are updated to be closer to each other for use in the next iteration. The algorithm stops if $\check{\tau}$ and $\hat{\tau}$ converge to each other within the tolerance δ. The inner algorithms, i.e., Algorithms 2, 3, 4, and 5, are presented in the following subsections.

Algorithm 1 Outer Algorithm for the Problem $\mathscr{P}_0$

Require: $\zeta, \tilde{R}^{\mathrm{UL}}, \tilde{R}^{\mathrm{DL}}, P_{\mathrm{t}}, \boldsymbol{h}_{b,u}, \sigma_u^2$, $b = 1, 2, \ldots, B$, $u = 0, 1, \ldots, U$

1: Set δ to be a small positive number
2: Obtain $\mathring{\mathcal{S}}$ by solving the problem $\mathring{\mathscr{P}}_1$
3: $(\check{\tau}, \hat{\tau}) \leftarrow (0, 1)$
4: **while** $|\check{\tau} - \hat{\tau}| > \delta$ **do**
5: $\quad\tau_{\mathrm{l}} \leftarrow \check{\tau} + (\hat{\tau} - \check{\tau})/3$
6: $\quad\tau_{\mathrm{r}} \leftarrow \hat{\tau} - (\hat{\tau} - \check{\tau})/3$
7: $\quad$**for** $\tau \in \{\tau_{\mathrm{l}}, \tau_{\mathrm{r}}\}$ **do**
8: $\quad\quad$**if** $\tau \in \mathcal{T}_{\mathrm{A}}(\mathring{\mathcal{S}})$ **then**
9: $\quad\quad\quad$**while** not converge nor reach max iteration **do**
10: $\quad\quad\quad\quad$Update $\boldsymbol{w}_u \forall u$ using Algorithm 2
11: $\quad\quad\quad\quad$Update $p_u \forall u$ using Algorithm 3
12: $\quad\quad\quad$**end while**
13: $\quad\quad\quad$Obtain $\mathcal{S}_\tau^*$ from $\{\boldsymbol{w}_u, p_u \forall u\}$
14: $\quad\quad$**else if** $\tau \in \mathcal{T}_{\mathrm{B}}(\mathring{\mathcal{S}})$ **then**
15: $\quad\quad\quad$**while** not converge nor reach max iteration **do**
16: $\quad\quad\quad\quad$Update $\boldsymbol{w}_u \forall u$ using Algorithm 4
17: $\quad\quad\quad\quad$Update $p_u \forall u$ using Algorithm 5
18: $\quad\quad\quad$**end while**
19: $\quad\quad\quad$Obtain $\mathcal{S}_\tau^*$ from $\{\boldsymbol{w}_u, p_u \forall u\}$
20: $\quad\quad$**else**
21: $\quad\quad\quad\mathcal{S}_\tau^* \leftarrow \mathring{\mathcal{S}}$
22: $\quad\quad$**end if**
23: $\quad\quad f(\mathcal{S}_\tau^*, \tau) \leftarrow \zeta \min\{\tau\tilde{R}^{\mathrm{UL}}, (1-\tau)\log_2(1+\gamma_0^{\mathrm{UL}}(\mathcal{S}_\tau^*))\} + (1-\zeta)\min\{\tau\tilde{R}^{\mathrm{DL}}, (1-\tau)\sum_{u=1}^{U}\log_2(1+\gamma_u^{\mathrm{DL}}(\mathcal{S}_\tau^*))\}$
24: $\quad$**end for**
25: $\quad$**if** $f(\mathcal{S}_{\tau_{\mathrm{l}}}^*, \tau_{\mathrm{l}}) < f(\mathcal{S}_{\tau_{\mathrm{r}}}^*, \tau_{\mathrm{r}})$ **then**
26: $\quad\quad\check{\tau} \leftarrow \tau_{\mathrm{l}}$ and $\tau^* \leftarrow \tau_{\mathrm{r}}$
27: $\quad$**else**
28: $\quad\quad\hat{\tau} \leftarrow \tau_{\mathrm{r}}$ and $\tau^* \leftarrow \tau_{\mathrm{l}}$
29: $\quad$**end if**
30: **end while**
Return: $\mathcal{S}_{\tau^*}^*, \tau^*$

B. Algorithms for Problem $\mathscr{P}_{1,\mathrm{A}}(\tau)$

The problem $\mathscr{P}_{1,\mathrm{A}}(\tau)$ is decomposed into two subproblems based on the block coordinate update method [79]. First, the BF vectors $\boldsymbol{w}_u \forall u$ defined in (16) are optimized for fixed common power levels. Then the common power levels $p_u \forall u$ are optimized for fixed BF vectors. Then the two subproblems, namely, $\mathscr{P}_{1,\mathrm{A}}^{\mathrm{BF}}(\tau, \{p_i\}_{i=0}^U)$ and $\mathscr{P}_{1,\mathrm{A}}^{\mathrm{PL}}(\tau, \{\boldsymbol{w}_i\}_{i=0}^U)$, are alternately updated in an iterative manner.

1) BF Optimization: First, the algorithm to solve the subproblem for BF design is explained here. For notational convenience, the effective channel vector from the gNBs to the uth UE (or satellite) with respect to p_j is defined as

$$\tilde{\boldsymbol{h}}_{u,j} \triangleq \Big[\sqrt{p_j}\boldsymbol{h}_{1,u}^{\mathrm{T}}, \sqrt{p_j}\boldsymbol{h}_{2,u}^{\mathrm{T}}, \ldots, \sqrt{p_j}\boldsymbol{h}_{B,u}^{\mathrm{T}}\Big]^{\mathrm{T}} \tag{18}$$

for $u, j = 0, 1, \ldots, U$. Using (18), the following function is also defined for $u = 0, 1, \ldots, U$,

$$f_u^{\mathrm{BF}}\big(\{\boldsymbol{w}_i\}_{i=0}^U\big) \triangleq \log_2\left(1 + \frac{\left|\tilde{\boldsymbol{h}}_{u,u}^\dagger \boldsymbol{w}_u\right|^2}{\sum_{\substack{j=0,\\ j\neq u}}^U \left|\tilde{\boldsymbol{h}}_{u,j}^\dagger \boldsymbol{w}_j\right|^2 + \sigma_u^2}\right) \quad (19)$$

which is a function of the vectors $\boldsymbol{w}_u, \forall u$ in (16). Substituting (19) into the problem $\mathscr{P}_{1,\mathrm{A}}(\tau)$, the subproblem for optimizing the BF vectors, $\boldsymbol{w}_u, \forall u$, is expressed for fixed $p_u, \forall u$ as

$$\begin{aligned} \mathscr{P}_{1,\mathrm{A}}^{\mathrm{BF}}\big(\tau, \{p_i\}_{i=0}^U\big): \quad \underset{\{\boldsymbol{w}_u \forall u\}}{\text{maximize}} \quad & \sum_{u=1}^U f_u^{\mathrm{BF}}\big(\{\boldsymbol{w}_i\}_{i=0}^U\big) \\ \text{subject to} \quad & f_0^{\mathrm{BF}}\big(\{\boldsymbol{w}_i\}_{i=0}^U\big) \geqslant \frac{\tau}{1-\tau}\tilde{R}^{\mathrm{UL}} \\ & \|\boldsymbol{w}_u\|^2 = 1, u = 0, 1, \ldots, U\,. \end{aligned}$$

To solve the non-convex problem $\mathscr{P}_{1,\mathrm{A}}^{\mathrm{BF}}\big(\tau, \{p_i\}_{i=0}^U\big)$, we find a local optimal solution that satisfies the Karush-Kuhn-Tucker (KKT) conditions [79]. The KKT conditions for the lower-level optimization can be necessary conditions for the upper-level optimization due to the nested structure of the problems. The Lagrangian function for the problem $\mathscr{P}_{1,\mathrm{A}}^{\mathrm{BF}}\big(\tau, \{p_i\}_{i=0}^U\big)$ is expressed by

$$\begin{aligned} \ell_{1,\mathrm{A}}^{\mathrm{BF}} = & \sum_{u=1}^U f_u^{\mathrm{BF}}\big(\{\boldsymbol{w}_i\}_{i=0}^U\big) - \mu\Big(\frac{\tau}{1-\tau}\tilde{R}^{\mathrm{UL}} - f_0^{\mathrm{BF}}\big(\{\boldsymbol{w}_i\}_{i=0}^U\big)\Big) \\ & + \sum_{u=0}^U \lambda_u\big(1 - \|\boldsymbol{w}_u\|^2\big) \end{aligned} \quad (20)$$

where $\mu \geqslant 0$ and λ_u are the KKT multipliers. First, the following relation is derived as a necessary condition using the stationarity, i.e., $(\partial \ell_{1,\mathrm{A}}^{\mathrm{BF}}/\partial \boldsymbol{w}_u) = 0 \forall u$,

$$\big(\boldsymbol{S}_u - \boldsymbol{T}_u\big)\boldsymbol{w}_u = \lambda_u \boldsymbol{w}_u \quad (21)$$

for $u = 0, 1, \ldots, U$, where $\boldsymbol{S}_u$ and $\boldsymbol{T}_u$ are defined as

$$\boldsymbol{S}_u \triangleq \begin{cases} \mu\tilde{\boldsymbol{H}}_{0,0} & \text{for } u = 0 \\ \tilde{\boldsymbol{H}}_{u,u} & \text{for } u \geqslant 1 \end{cases} \quad (22a)$$

$$\boldsymbol{T}_u \triangleq \begin{cases} \sum_{j=1}^U \gamma_j \tilde{\boldsymbol{H}}_{j,0} & \text{for } u = 0 \\ \sum_{j=1, j\neq u}^U \gamma_j \tilde{\boldsymbol{H}}_{j,u} + \mu\gamma_0 \tilde{\boldsymbol{H}}_{0,u} & \text{for } u \geqslant 1 \end{cases} \quad (22b)$$

with

$$\tilde{\boldsymbol{H}}_{j,u} \triangleq \frac{1}{\rho_j \ln 2}\tilde{\boldsymbol{h}}_{j,u}\tilde{\boldsymbol{h}}_{j,u}^\dagger \quad (23a)$$

$$\rho_j \triangleq \sum_{i=0}^U \left|\tilde{\boldsymbol{h}}_{j,i}^\dagger \boldsymbol{w}_i\right|^2 + \sigma_j^2 \quad (23b)$$

$$\gamma_j \triangleq \frac{\left|\tilde{\boldsymbol{h}}_{j,j}^\dagger \boldsymbol{w}_j\right|^2}{\sum_{i=0, i\neq j}^U \left|\tilde{\boldsymbol{h}}_{j,i}^\dagger \boldsymbol{w}_i\right|^2 + \sigma_j^2}\,. \quad (23c)$$

In (21), the BF vector $\boldsymbol{w}_u$ can be chosen to be one of the eigenvectors of the matrix $\boldsymbol{S}_u - \boldsymbol{T}_u$. To find the best BF vector, the variables in (21) are interpreted as follows. From (22), $\boldsymbol{S}_u$ corresponds to the desired channel component, while $\boldsymbol{T}_u$ can be seen as the weighted sum of leakage components from the uth UE or satellite to the other nodes. In $\boldsymbol{T}_u$, the leakage to the jth node from the uth node is weighted by the ratio between the SINR and the received signal strength at the jth node, i.e., γ_j/ρ_j. From this observation, we combine the two conditions: the stationarity in (21) and the primal feasibility $\|\boldsymbol{w}_u\|^2 = 1$ to derive $\boldsymbol{w}_u^\dagger\big(\boldsymbol{S}_u - \boldsymbol{T}_u\big)\boldsymbol{w}_u = \lambda_u$. The eigenvalue λ_u can be considered the difference between the desired channel power and the weighted sum of the leakage powers. Hence, We find the best BF vector $\boldsymbol{w}_u$ that maximizes λ_u among the eigenvectors. Since $\boldsymbol{S}_u$ and $\boldsymbol{T}_u$ are coupled by $\boldsymbol{w}_u$, we use an iterative update method for optimizing $\boldsymbol{w}_u$. Specifically, for each iteration of the algorithm, $\boldsymbol{w}_u$ is updated by solving the following problem for given μ, ρ_u, and $\gamma_u \forall u$

$$\begin{aligned} \underset{\boldsymbol{w}_u}{\text{maximize}} \quad & \boldsymbol{w}_u^\dagger\big(\boldsymbol{S}_u - \boldsymbol{T}_u\big)\boldsymbol{w}_u & (24a) \\ \text{subject to} \quad & \|\boldsymbol{w}_u\|^2 = 1\,. & (24b) \end{aligned}$$

This problem can be solved by calculating the dominant eigenvector of the symmetric matrix $\boldsymbol{S}_u - \boldsymbol{T}_u$, which is given by using $\rho_u \forall u$ of the previous iteration. Define the eigenvalue decomposition as $\boldsymbol{S}_u - \boldsymbol{T}_u = \boldsymbol{U}_u \boldsymbol{\Sigma}_u \boldsymbol{U}_u^\dagger$ with the eigenvectors in $\boldsymbol{U}_u \triangleq [\boldsymbol{u}_{u,1}, \boldsymbol{u}_{u,2}, \cdots, \boldsymbol{u}_{u,BM}]$ and the eigenvalues in the diagonal matrix $\boldsymbol{\Sigma}_u$ in descending order. Then the solution to the problem in (24a) and (24b) is given by

$$\boldsymbol{w}_u = \frac{\boldsymbol{u}_{u,1}}{\|\boldsymbol{u}_{u,1}\|}\,. \quad (25)$$

Using (25), an optimal μ can be found by the bisection method to satisfy the complementary slackness, i.e., $\mu\big[(\tau/1-\tau)\tilde{R}^{\mathrm{UL}} - f_0^{\mathrm{BF}}\big(\{\boldsymbol{w}_i\}_{i=0}^U\big)\big] = 0$, under the primal feasibility condition, i.e., $f_0^{\mathrm{BF}}\big(\{\boldsymbol{w}_i\}_{i=0}^U\big) \geqslant (\tau/1-\tau)\tilde{R}^{\mathrm{UL}}$. The algorithm to solve $\mathscr{P}_{1,\mathrm{A}}^{\mathrm{BF}}\big(\tau, \{p_i\}_{i=0}^U\big)$ is summarized in Algorithm 2. The value $\check{\mu}$ in Step 1 is chosen as a large positive number so that an optimal $\mu \geqslant 0$, which satisfies the primal feasibility of the inequality constraint in $\mathscr{P}_{1,\mathrm{A}}^{\mathrm{BF}}\big(\tau, \{p_i\}_{i=0}^U\big)$, can be found.

2) Power Level Optimization: The algorithm for the second subproblem for power level optimization is explained in the following. First, we define the effective channel gain for given BF vectors as

$$g_{u,j} \triangleq \left|\sum_{b=1}^B \boldsymbol{h}_{b,u}^\dagger \boldsymbol{w}_{b,j}\right|^2 = \left|\boldsymbol{h}_u^\dagger \boldsymbol{w}_j\right|^2 \quad (26)$$

for $u, j = 0, 1, \ldots, U$, where $\boldsymbol{h}_u$ is defined in (9). Using (26), the following function is also defined for $u = 0, 1, \ldots, U$,

$$f_u^{\mathrm{PL}}\big(\{p_i\}_{i=0}^U\big) \triangleq \log_2\left(1 + \frac{g_{u,u}\, p_u}{\sum_{j=0, j\neq u}^U g_{u,j}\, p_j + \sigma_u^2}\right) \quad (27)$$

which is a function of $p_u \forall u$ in (16). Substituting (27) into the problem $\mathscr{P}_{1,\mathrm{A}}(\tau)$, the subproblem for optimizing the common power levels $p_u \forall u$ is expressed for fixed $\boldsymbol{w}_u \forall u$ as

$$\begin{aligned} \mathscr{P}_{1,\mathrm{A}}^{\mathrm{PL}}\big(\tau, \{\boldsymbol{w}_i\}_{i=0}^U\big): \quad \underset{\{p_u \geqslant 0 \forall u\}}{\text{maximize}} \quad & \sum_{u=1}^U f_u^{\mathrm{PL}}\big(\{p_i\}_{i=0}^U\big) \\ \text{subject to} \quad & f_0^{\mathrm{PL}}\big(\{p_i\}_{i=0}^U\big) \geqslant \frac{\tau}{1-\tau}\tilde{R}^{\mathrm{UL}} \\ & \sum_{u=0}^U \|\boldsymbol{w}_{b,u}\|^2 p_u \leqslant P_{\mathrm{t}} \forall b\,. \end{aligned}$$

Algorithm 2 BF Optimization for the Problem $\mathscr{P}_{1,\mathrm{A}}^{\mathrm{BF}}\big(\tau, \{p_i\}_{i=0}^U\big)$

Require:$\tau, \tilde{R}^{\mathrm{UL}}, \boldsymbol{h}_{b,u}, p_u, \sigma_u^2\,\forall b, u$
Set $\breve{\mu}$ to be a positive number
$\boldsymbol{w}_u \leftarrow \tilde{\boldsymbol{h}}_{u,u}/\|\tilde{\boldsymbol{h}}_{u,u}\|\forall u$ using (18)
while $\boldsymbol{w}_u, \forall u$ does not converge within max iteration **do**
  Update $\big\{\tilde{\boldsymbol{H}}_{j,u}, \rho_j, \gamma_j \forall j, u\big\}$
  $(\breve{\mu}, \hat{\mu}) \leftarrow (0, \breve{\mu})$
  while μ does not converge **do**
    $\mu \leftarrow (\breve{\mu} + \hat{\mu})/2$
    Update $\boldsymbol{S}_u$ and $\boldsymbol{T}_u \forall u$ using (22)
    Update $\boldsymbol{w}_u \forall u$ using (25)
    if $\log_2\Big(1+\frac{|\tilde{\boldsymbol{h}}_{0,0}^\dagger \boldsymbol{w}_0|^2}{\sum_{j=1}^U |\tilde{\boldsymbol{h}}_{0,j}^\dagger \boldsymbol{w}_j|^2+\sigma_0^2}\Big) > \frac{\tau}{1-\tau}\tilde{R}^{\mathrm{UL}}$ **then**
      $\hat{\mu} \leftarrow \mu$
    else
      $\breve{\mu} \leftarrow \mu$
    end if
  end while
end while
Return: $\boldsymbol{w}_u \forall u$

The Lagrangian function for $\mathscr{P}_{1,\mathrm{A}}^{\mathrm{PL}}\big(\tau, \{\boldsymbol{w}_i\}_{i=0}^U\big)$ is given by

$$\ell_{1,\mathrm{A}}^{\mathrm{PL}} = \sum_{u=1}^U f_u^{\mathrm{PL}}\big(\{p_i\}_{i=0}^U\big) - \eta\Big(\frac{\tau}{1-\tau}\tilde{R}^{\mathrm{UL}} - f_0^{\mathrm{PL}}\big(\{p_i\}_{i=0}^U\big)\Big) - \sum_{b=1}^B \nu_b\Big(\sum_{u=0}^U \|\boldsymbol{w}_{b,u}\|^2 p_u - P_{\mathrm{t}}\Big) \tag{28}$$

where $\eta \geqslant 0$ and $\nu_b \geqslant 0$ are the KKT multipliers. From the stationarity, i.e., $\partial \ell_{1,\mathrm{A}}^{\mathrm{PL}}/\partial p_u = 0 \forall u$, and the feasibility, i.e., $p_u \geqslant 0 \forall u$, we derive the following relations,

$$p_u = \begin{cases} \Big[\dfrac{\eta}{t_0 + \sum_{b=1}^B \nu_b \|\boldsymbol{w}_{b,0}\|^2 \ln 2} - q_0\Big]^+ & \text{if } u = 0 \\ \Big[\dfrac{1}{t_u + \eta s_u + \sum_{b=1}^B \nu_b \|\boldsymbol{w}_{b,u}\|^2 \ln 2} - q_u\Big]^+ & \text{if } u \geqslant 1 \end{cases} \tag{29}$$

where

$$q_u \triangleq \Big(\sum_{i=0, i\neq u}^U g_{u,i}\, p_i + \sigma_u^2\Big)/g_{u,u} \tag{30a}$$

$$t_u \triangleq \sum_{j=0, j\neq u}^U g_{j,u}\gamma_j/\rho_j \tag{30b}$$

$$s_u \triangleq g_{0,u}\gamma_0/\rho_0\,. \tag{30c}$$

In (29), the function $[x]^+ \triangleq \max(x, 0)$ is used to consider the non-negativity of p_u. In (30), ρ_j and γ_j can be expressed as $\rho_j = \sum_{i=0}^U g_{j,i}\, p_i + \sigma_j^2$ and $\gamma_j = g_{j,j}\, p_j/(\sum_{i=0, i\neq j}^U g_{j,i}\, p_i + \sigma_j^2)$, respectively, using (23) and (26).

In (29), p_u monotonically increases with η when $u = 0$ and decreases when $u \geqslant 1$ for given other variables. In other words, the function $f_0^{\mathrm{PL}}\big(\{p_i\}_{i=0}^U\big)$ in the first constraint monotonically increases with η. Hence, for a given set $\{\nu_b \forall b\}$, an optimal η is found by the bisection search to satisfy the complementary slackness, i.e., $\eta\big[(\tau/1-\tau)\tilde{R}^{\mathrm{UL}} - f_0^{\mathrm{PL}}\big(\{p_i\}_{i=0}^U\big)\big] = 0$, under the primal feasibility condition, i.e., $f_0^{\mathrm{PL}}\big(\{p_i\}_{i=0}^U\big) \geqslant (\tau/1-\tau)\tilde{R}^{\mathrm{UL}}$. Similarly, p_u in (29) is a monotonic function of ν_b for given other variables. Hence, for each iteration, optimal $\nu_b \forall b$ are found by the multi-dimensional bisection search to satisfy that $\nu_b\big[\sum_{u=0}^U \|\boldsymbol{w}_{b,u}\|^2 p_u - P_{\mathrm{t}}\big] = 0$ under $\sum_{u=0}^U \|\boldsymbol{w}_{b,u}\|^2 p_u \leqslant P_{\mathrm{t}}\,\forall b$. The power level optimization algorithm to solve the problem $\mathscr{P}_{1,\mathrm{A}}^{\mathrm{PL}}\big(\tau, \{\boldsymbol{w}_i\}_{i=0}^U\big)$ is summarized in Algorithm 3.

Algorithm 3 Power Level Optimization for the Problem $\mathscr{P}_{1,\mathrm{A}}^{\mathrm{PL}}\big(\tau, \{\boldsymbol{w}_i\}_{i=0}^U\big)$

Require:$\tau, \tilde{R}^{\mathrm{UL}}, P_{\mathrm{t}}, \boldsymbol{w}_{b,u}, \boldsymbol{h}_{b,u}, \sigma_u^2\,\forall b, u$
Set $\breve{\eta}$ and $\breve{\nu}$ to be positive numbers
Initialize $p_u \forall u$ with equal power allocation
Initialize $\nu_b \forall b$ with $\breve{\nu}$
while $\{p_u \forall u\}$ does not converge within max iteration **do**
  Update $\{q_u, t_u, s_u \forall u\}$ using (30)
  $(\breve{\eta}, \hat{\eta}) \leftarrow (0, \breve{\eta})$
  while η does not converge **do**
    $\eta \leftarrow (\breve{\eta} + \hat{\eta})/2$
    Update $p_u \forall u$ using (29)
    if $\log_2\Big(1+\frac{g_{0,0}\, P_0}{\sum_{j=1}^U g_{0,j}\, p_j + \sigma_0^2}\Big) > \frac{\tau}{1-\tau}\tilde{R}^{\mathrm{UL}}$ **then**
      $\hat{\eta} \leftarrow \eta$
    else
      $\breve{\eta} \leftarrow \eta$
    end if
  end while
  $(\breve{\nu}_b, \hat{\nu}_b) \leftarrow (0, \breve{\nu})\forall b$
  while $\{\nu_b\,\forall b\}$ does not converge within max iteration **do**
    $\nu_b \leftarrow (\breve{\nu}_b + \hat{\nu}_b)/2 \forall b$
    Update $p_u \forall u$ using (29)
    for $b = 1, 2, \ldots, B$ **do**
      if $\sum_{u=0}^U \|\boldsymbol{w}_{b,u}\|^2 p_u > P_{\mathrm{t}}$ **then**
        $\breve{\nu}_b \leftarrow \nu_b$
      else
        $\hat{\nu}_b \leftarrow \nu_b$
      end if
    end for
  end while
end while
Return: $p_u \forall u$

C. Algorithms for Problem $\mathscr{P}_{1,\mathrm{B}}(\tau)$

Following a similar design approach with that for $\mathscr{P}_{1,\mathrm{A}}\big(\tau\big)$ in Sec. IV-B, the problem $\mathscr{P}_{1,\mathrm{B}}\big(\tau\big)$ is decomposed into the two subproblems, denoted by $\mathscr{P}_{1,\mathrm{B}}^{\mathrm{BF}}\big(\tau, \{p_i\}_{i=0}^U\big)$ and $\mathscr{P}_{1,\mathrm{B}}^{\mathrm{PL}}\big(\tau, \{\boldsymbol{w}_i\}_{i=0}^U\big)$. Then these subproblems are alternately solved in an iterative algorithm.

1) BF Optimization: Substituting (19) into the problem $\mathscr{P}_{1,\mathrm{B}}\big(\tau\big)$, the subproblem for optimizing $\boldsymbol{w}_u \forall u$ can be expressed for fixed common power levels $p_u \forall u$ as

$$\mathscr{P}_{1,\mathrm{B}}^{\mathrm{BF}}\big(\tau, \{p_i\}_{i=0}^U\big): \underset{\{\boldsymbol{w}_u \forall u\}}{\text{maximize}}\ f_0^{\mathrm{BF}}\big(\{\boldsymbol{w}_i\}_{i=0}^U\big) \quad \text{subject to}\ \sum_{u=1}^U f_u^{\mathrm{BF}}\big(\{\boldsymbol{w}_i\}_{i=0}^U\big) \geqslant \frac{\tau}{1-\tau}\tilde{R}^{\mathrm{DL}}, \ \|\boldsymbol{w}_u\|^2 = 1, u = 0, 1, \ldots, U\,.$$

Algorithm 4 BF Optimization for the Problem $\mathscr{P}_{1,\mathrm{B}}^{\mathrm{BF}}\big(\tau,\{p_i\}_{i=0}^{U}\big)$

Require: $\tau, \tilde{R}^{\mathrm{DL}}, \boldsymbol{h}_{b,u}, p_u, \sigma_u^2\,\forall b,u$
Set $\breve{\mu}$ to be a positive number
$\boldsymbol{w}_u \leftarrow \tilde{\boldsymbol{h}}_{u,u}/\|\tilde{\boldsymbol{h}}_{u,u}\|\forall u$ using (18)
while $\boldsymbol{w}_u\forall u$ does not converge within max iteration **do**
  Update $\{\tilde{\boldsymbol{H}}_{j,u}, \rho_j, \gamma_j \forall j,u\}$
  $(\breve{\mu},\hat{\mu}) \leftarrow (0,\breve{\mu})$
  while $\bar{\mu}$ does not converge **do**
    $\bar{\mu} \leftarrow (\breve{\mu}+\hat{\mu})/2$
    Update $\bar{\boldsymbol{S}}_u$ and $\bar{\boldsymbol{T}}_u\forall u$ using (33)
    Update $\boldsymbol{w}_u\forall u$ using (34)
    if $\sum_{u=1}^{U}\log_2\Big(1+\frac{|\tilde{\boldsymbol{h}}_{u,u}^{\dagger}\boldsymbol{w}_u|^2}{\sum_{\substack{j=0,\\ j\neq u}}^{U}|\tilde{\boldsymbol{h}}_{u,j}^{\dagger}\boldsymbol{w}_j|^2+\sigma_u^2}\Big) > \frac{\tau}{1-\tau}\tilde{R}^{\mathrm{DL}}$ **then**
      $\hat{\mu} \leftarrow \bar{\mu}$
    else
      $\breve{\mu} \leftarrow \bar{\mu}$
    end if
  end while
end while
Return: $\boldsymbol{w}_u\forall u$

To find the KKT conditions, the Lagrangian function for the problem $\mathscr{P}_{1,\mathrm{B}}^{\mathrm{BF}}(\tau,\{p_i\}_{i=0}^{U})$ is expressed by

$$\ell_{1,\mathrm{B}}^{\mathrm{BF}} = f_0^{\mathrm{BF}}\big(\{\boldsymbol{w}_i\}_{i=0}^{U}\big) - \bar{\mu}\Big(\frac{\tau}{1-\tau}\tilde{R}^{\mathrm{DL}} - \sum_{u=1}^{U} f_u^{\mathrm{BF}}\big(\{\boldsymbol{w}_i\}_{i=0}^{U}\big)\Big) + \sum_{u=0}^{U}\bar{\lambda}_u\big(1-\|\boldsymbol{w}_u\|^2\big) \tag{31}$$

where $\bar{\mu} \geqslant 0$ and $\bar{\lambda}_u$ are the KKT multipliers. Similarly to the procedure from (21) to (24b), the stationarity, i.e., $\partial\ell_{1,\mathrm{B}}^{\mathrm{BF}}/\partial\boldsymbol{w}_u = 0\forall u$, and the primal feasibility, i.e., $\|\boldsymbol{w}_u\|^2 = 1\forall u$, lead to an update problem at each iteration of the algorithm. This is expressed for given $\bar{\mu}$, ρ_u, and $\gamma_u\forall u$ as

$$\underset{\boldsymbol{w}_u}{\text{maximize}} \quad \boldsymbol{w}_u^{\dagger}\big(\bar{\boldsymbol{S}}_u - \bar{\boldsymbol{T}}_u\big)\boldsymbol{w}_u \tag{32a}$$

$$\text{subject to} \quad \|\boldsymbol{w}_u\|^2 = 1 \tag{32b}$$

where $\bar{\boldsymbol{S}}_u$ and $\bar{\boldsymbol{T}}_u$ are defined differently from $\boldsymbol{S}_u$ and $\boldsymbol{T}_u$ in (22), respectively, as

$$\bar{\boldsymbol{S}}_u \triangleq \begin{cases} \tilde{\boldsymbol{H}}_{0,0} & \text{for } u=0 \\ \bar{\mu}\tilde{\boldsymbol{H}}_{u,u} & \text{for } u \geqslant 1 \end{cases} \tag{33a}$$

$$\bar{\boldsymbol{T}}_u \triangleq \begin{cases} \bar{\mu}\sum_{j=1}^{U}\gamma_j\tilde{\boldsymbol{H}}_{j,0} & \text{for } u=0 \\ \bar{\mu}\sum_{\substack{j=1,\\ j\neq u}}^{U}\gamma_j\tilde{\boldsymbol{H}}_{j,u} + \gamma_0\tilde{\boldsymbol{H}}_{0,u} & \text{for } u \geqslant 1\,. \end{cases} \tag{33b}$$

The definitions of $\tilde{\boldsymbol{H}}_{j,u}$ and γ_j in (33) are given in (23). As observed in (24a), the objective function in (32a) also means the difference between the desired channel power and the weighted sum of the leakage powers. The solution to the problem in (32) is given by

$$\boldsymbol{w}_u = \frac{\bar{\boldsymbol{u}}_{u,1}}{\|\bar{\boldsymbol{u}}_{u,1}\|} \tag{34}$$

Algorithm 5 Power Level Optimization for the Problem $\mathscr{P}_{1,\mathrm{B}}^{\mathrm{PL}}\big(\tau,\{\boldsymbol{w}_i\}_{i=0}^{U}\big)$

Require: $\tau, \tilde{R}^{\mathrm{DL}}, P_{\mathrm{t}}, \boldsymbol{w}_{b,u}, \boldsymbol{h}_{b,u}, \sigma_u^2\,\forall b,u$
Set $\breve{\eta}$ and $\breve{\nu}$ to be positive numbers
Initialize $p_u\forall u$ with equal power allocation
Initialize $\bar{\nu}_b\forall b$ with $\breve{\nu}$
while $\{p_u\forall u\}$ does not converge within max iteration **do**
  Update $\{\bar{q}_u, \bar{t}_u, \bar{s}_u\forall u\}$ using (37)
  $(\breve{\eta},\hat{\eta}) \leftarrow (0,\breve{\eta})$
  while $\bar{\eta}$ does not converge **do**
    $\bar{\eta} \leftarrow (\breve{\eta}+\hat{\eta})/2$
    Update $p_u\forall u$ using (36)
    if $\sum_{u=1}^{U}\log_2\Big(1+\frac{g_{u,u}\,p_u}{\sum_{\substack{j=0,\\ j\neq u}}^{U}g_{u,j}p_j+\sigma_u^2}\Big) > \frac{\tau}{1-\tau}\tilde{R}^{\mathrm{DL}}$ **then**
      $\hat{\eta} \leftarrow \bar{\eta}$
    else
      $\breve{\eta} \leftarrow \bar{\eta}$
    end if
  end while
  $(\breve{\nu}_b,\hat{\nu}_b) \leftarrow (0,\breve{\nu})\forall b$
  while $\{\bar{\nu}_b\,\forall b\}$ does not converge within max iteration **do**
    $\bar{\nu}_b \leftarrow (\breve{\nu}_b+\hat{\nu}_b)/2\forall b$
    Update $p_u\forall u$ using (36)
    for $b=1,2,\ldots,B$ **do**
      if $\sum_{u=0}^{U}\|\boldsymbol{w}_{b,u}\|^2 p_u > P_{\mathrm{t}}$ **then**
        $\breve{\nu}_b \leftarrow \bar{\nu}_b$
      else
        $\hat{\nu}_b \leftarrow \bar{\nu}_b$
      end if
    end for
  end while
end while
Return: $p_u\forall u$

where $\bar{\boldsymbol{u}}_{u,1}$ is the dominant eigenvector of the matrix $\bar{\boldsymbol{S}}_u - \bar{\boldsymbol{T}}_u$. Similarly to Algorithm 2, $\bar{\mu}$ is found to satisfy the complementary slackness and the primal feasibility. The algorithm to solve $\mathscr{P}_{1,\mathrm{B}}^{\mathrm{BF}}\big(\tau,\{p_i\}_{i=0}^{U}\big)$ is summarized in Algorithm 4.

2) Power Level Optimization: Substituting (27) into the problem $\mathscr{P}_{1,\mathrm{B}}\big(\tau\big)$, the subproblem for optimizing the common power levels $p_u\forall u$ is expressed for fixed $\boldsymbol{w}_u\forall u$ as

$$\mathscr{P}_{1,\mathrm{B}}^{\mathrm{PL}}\big(\tau,\{\boldsymbol{w}_i\}_{i=0}^{U}\big)\colon \underset{\{p_u\geqslant 0\forall u\}}{\text{maximize}}\ f_0^{\mathrm{PL}}\big(\{p_i\}_{i=0}^{U}\big)$$
$$\text{subject to} \ \sum_{u=1}^{U} f_u^{\mathrm{PL}}\big(\{p_i\}_{i=0}^{U}\big) \geqslant \frac{\tau}{1-\tau}\tilde{R}^{\mathrm{DL}}$$
$$\sum_{u=0}^{U}\|\boldsymbol{w}_{b,u}\|^2 p_u \leqslant P_{\mathrm{t}}\forall b\,.$$

The Lagrangian function for $\mathscr{P}_{1,\mathrm{B}}^{\mathrm{PL}}\big(\tau,\{\boldsymbol{w}_i\}_{i=0}^{U}\big)$ is given by

$$\ell_{1,\mathrm{B}}^{\mathrm{PL}} = f_0^{\mathrm{PL}}\big(\{p_i\}_{i=0}^{U}\big) - \bar{\eta}\Big(\frac{\tau}{1-\tau}\tilde{R}^{\mathrm{DL}} - \sum_{u=1}^{U} f_u^{\mathrm{PL}}\big(\{p_i\}_{i=0}^{U}\big)\Big) - \sum_{b=1}^{B}\bar{\nu}_b\Big(\sum_{u=0}^{U}\|\boldsymbol{w}_{b,u}\|^2 p_u - P_{\mathrm{t}}\Big) \tag{35}$$

where $\bar{\eta} \geqslant 0$ and $\bar{\nu}_b \geqslant 0$ are the KKT multipliers. From the stationarity, i.e., $(\partial\ell_{1,\mathrm{B}}^{\mathrm{PL}}/\partial p_u) = 0\forall u$, and the feasibility, i.e.,

$p_u \geqslant 0 \forall u$, we derive the following:

$$p_u = \begin{cases} \left[\dfrac{1}{\bar{\eta}\bar{t}_0 + \sum_{b=1}^{B} \bar{\nu}_b \|\boldsymbol{w}_{b,0}\|^2 \ln 2} - \bar{q}_{0,u} \right]^+ & \text{if } u = 0 \\ \left[\dfrac{\bar{\eta}}{\bar{s}_u + \bar{\eta}\bar{t}_u + \sum_{b=1}^{B} \bar{\nu}_b \|\boldsymbol{w}_{b,u}\|^2 \ln 2} - \bar{q}_{u,u} \right]^+ & \text{if } u \geqslant 1 \end{cases} \tag{36}$$

where

$$\bar{q}_{j,u} \triangleq \Big(\sum_{i=0, i\neq u}^{U} g_{j,i}\, p_i + \sigma_j^2 \Big) / g_{j,u} \tag{37a}$$

$$\bar{t}_u \triangleq \sum_{j=1, j\neq u}^{U} \gamma_j g_{j,u} / \rho_j \tag{37b}$$

$$\bar{s}_u \triangleq \gamma_0 g_{0,u} / \rho_0 \,. \tag{37c}$$

The definitions of ρ_j and γ_j are given in (30). The multipliers $\bar{\eta}$ and $\bar{\nu}_b$ are found to satisfy the complementary slackness and the primal feasibility similarly to the approach in Algorithm 3. The power level optimization algorithm to solve the problem $\mathscr{P}_{1,\mathrm{B}}^{\mathrm{PL}}\big(\tau, \{\boldsymbol{w}_i\}_{i=0}^{U}\big)$ is summarized in Algorithm 5.

V. Simulation Results

In this section, performances of the proposed ITSN are numerically presented in terms of the achievable rates in both UL and DL. In particular, the UL-DL rate region of the proposed scheme is compared with the performances of the baseline schemes, including the classical out-of-band backhauling, in-band backhauling, and the outer bound of the in-band backhauling with reverse TDD.

A. Simulation Setup

We consider two 3GPP scenarios for simulations: Urban micro (UMi) scenario (Street canyon) with *Ka*-band (at 30 GHz) and Rural scenario with *S*-band (at 4 GHz). The network parameters for the different scenarios are presented in Table I. A shorter inter-gNB distance is set for the UMi scenario with high center frequency, i.e., 30 GHz, while a longer one is for the Rural scenario with low center frequency, i.e., 4 GHz [65], [66]. The random parameters of large-scale and small-scale channels are realized for given positions of the nodes using the 3GPP non-terrestrial and terrestrial models in [65] and [66] as described in Sec. II-C. The maximum values for searching the KKT multipliers are set as $\check{\mu} = 10^5, \check{\eta} = 10$, and $\check{\nu} = 10$ in the algorithms.

1) Parameters for the Satellite: The GEO satellite is located at the altitude of $h_{\mathrm{SAT}} = 35,786$ km. The elevation angle between the satellite and the origin of the terrestrial network is set to be 50° unless otherwise noted. Then $d_{b,0}$ and α_b are calculated by using the relative locations of the bth gNB from the origin based on the coordinate system in [65]. The satellite is equipped with an antenna aperture, of which diameter is set to be 3.3 m, looking at the origin of the terrestrial network with the maximum beam gain of 58.5 dBi [2]. The antenna gain of the satellite is determined by the beam pattern function with respect to the elevation angle between the satellite and each gNB. To be specific, the beam pattern model in [65, Sec. 6.4.1] is used for $G_{b,0}^{\mathrm{TX}}$ in DL and $G_{b,0}^{\mathrm{RX}}$ in UL, which depend on the location of the bth gNB. The noise power spectral density at the satellite is set to be -169 dBm/Hz. The transmit power of the satellite is set to be $P_0' = 40$ or 50 dBm.

TABLE I
Simulation Parameters for Different Scenarios

Parameter	Value	
	UMi scenario	Rural scenario
Inter-gNB distance	250 m	1250 m
gNB height	10 m	35 m
UE height	1.5 m	1.5 m
f_{c}	30 GHz	4 GHz
Bandwidth	10 MHz	1 MHz
gNB power limit P_{t}	$27, 35, 43$ dBm	
UE power P_u'	23 dBm $\forall u = 1, 2, \ldots, U$	
Satellite power P_0'	$40, 50$ dBm	

2) Parameters for the Terrestrial Network: In the terrestrial network, $B = 4$ gNBs are located at $(D/2, D/2)$, $(-D/2, D/2)$, $(-D/2, -D/2)$, and $(-D/2, -D/2)$ of the xy-plane, where D is the inter-gNB distance. The locations of $U = 2$ UEs are given at $(100, 30)$ and $(-40, -90)$ for UMi scenario and $(500, 150)$ and $(-2000, -450)$ for Rural scenario, respectively. The gNBs are equipped with a cylindrical array, which consists of M_{L} circular arrays, each with M_{C} elements such that $M = M_{\mathrm{C}} \times M_{\mathrm{L}}$. The antenna elements of the gNBs and UEs are assumed to have an omnidirectional radiation pattern. The noise power spectral densities are set to be -166 dBm/Hz and -165 dBm/Hz at the gNBs and UEs, respectively. The transmit power of each gNB is set to be $P_{\mathrm{t}} = 27, 35$, or 43 dBm, while that of each UE is set to be $P_u' = 23$ dBm for $u = 1, 2, \ldots, U$.

B. Baseline Performances

For comparison, we plot three baseline schemes which are explained as follows. First, an outer bound of the rate region for the reverse TDD is presented, which assumes that the maximum transmit power P_{t} is used with optimized BF in both access and backhaul links separately with no interference between access and backhaul. Specifically, for calculating the upper bound of the backhaul UL rate, each BF vector $\boldsymbol{w}_{b,0}$ is matched to $\boldsymbol{h}_{b,0}$ with $\|\boldsymbol{w}_{b,0}\|^2 P_{b,0} = P_{\mathrm{t}} \forall b$. For calculating the upper bound of the access DL sum rate, the vectors $\{\boldsymbol{w}_{b,u}, u \geqslant 1, b \geqslant 1\}$ are optimized to maximize the weighted sum rate of the access DL under per-gNB power constraint P_{t} using the solution in [76]. The upper bounds for the backhaul DL and access UL are obtained by separately solving the problem in (11) without any interference between the backhaul DL and access UL. The outer bound of the end-to-end rate region is plotted using the upper bounds for UL and DL with varying τ. Second, the classical out-of-band backhauling with TDD in Fig. 1(a) is compared as a baseline performance. For this scheme, the rate region is determined by varying the ratio between the total UL period and total DL period while optimizing time division ratios between the access UL and backhaul UL and between the access DL and backhaul DL to maximize each end-to-end rates. Third, an in-band

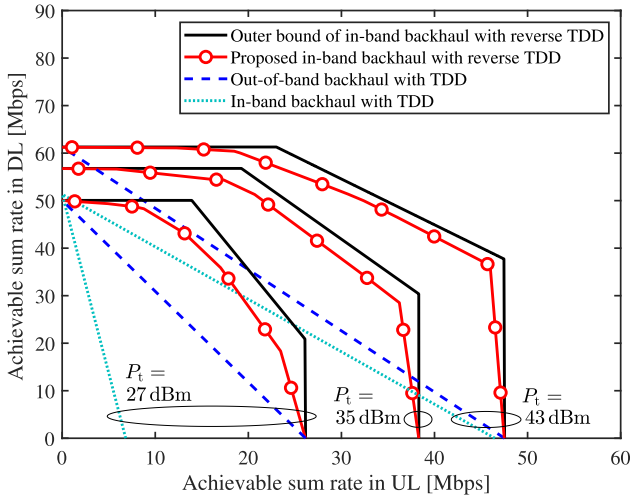

(a) UMi scenario at 30 GHz

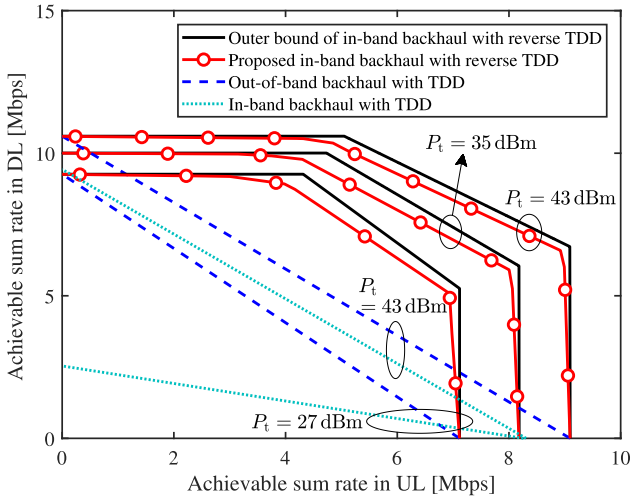

(b) Rural scenario at 4 GHz

Fig. 5. UL-DL rate region with different P_t for a channel realization: $P_0' = 50$ dBm, $M = 8 \times 2$.

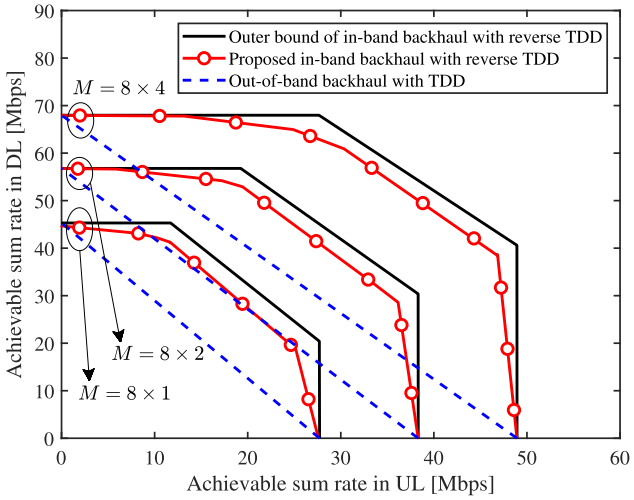

(a) UMi scenario at 30 GHz

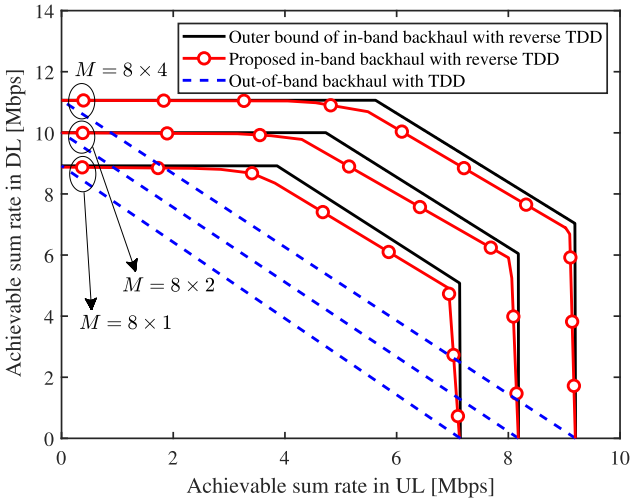

(b) Rural scenario at 4 GHz

Fig. 6. UL-DL rate region with different M for a channel realization: $P_0' = 50$ dBm, $P_t = 35$ dBm.

backhauling with TDD in Fig. 1(c) is compared to validate the benefits from the reverse TDD in the context of ITSN. For a fair comparison, the gNBs are assumed to be half-duplex systems. To enable the transmission configuration in Fig. 1(c), a half of the gNBs is dedicated to backhaul transmission, and the other half is dedicated to access transmission. In this case, additional interference occurs between the satellite and UEs as well as among the gNBs. The transmit BF vectors and the power allocation vectors for the gNBs are optimized using the existing algorithm in [76], while the receive BF vectors for the gNBs are optimized similarly with (11) by adjusting the interference terms. The rate region is obtained by varying τ from 0 to 1.

C. Performance Evaluation

Fig. 5 presents the UL-DL rate regions for different P_t in UMi and Rural scenarios, which can be obtained by solving $\mathscr{P}_0$ with varying ζ from zero to one. Each rate region consists of the set of the end-to-end UL rate and DL rate pairs. The proposed ITSN with in-band backhauling covers a significantly larger area of the rate region with a better trade-off compared to the out-of-band backhauling with TDD and the in-band backhauling with TDD. Moreover, the rate region of the proposed ITSN approaches the outer bound. Note that the proposed scheme may not achieve the exact outer bound at each axis, e.g., $\zeta = 0$ and $\zeta = 1$, because of the interference from the satellite and the UEs, which use the fixed transmit powers. However, the proposed scheme exploits the receive BF with antenna arrays at the gNBs to mitigate the interference so that the achievable rate region is close to the outer bound. In addition, it can be seen that the rate region enlarges in both axes as P_t increases because a larger P_t can improve both the UL and DL by adjusting τ. In particular, the impact of increasing P_t is significant in a low power regime of the UMi scenario at 30 GHz.

Fig. 6 shows the effect of increasing M on the UL-DL rate region. Since M directly affects both the receive and transmit BF gains of the gNBs at time slot 1 and time slot 2, respectively, the rate region enlarges in both axes as M increases. Compared to the case with $P_t = 45$ dBm and $M = 8 \times 2$ in Fig. 5(a), the case with $P_t = 35$ dBm and $M = 8 \times 4$ in Fig. 6(a) achieves a remarkably higher rate in

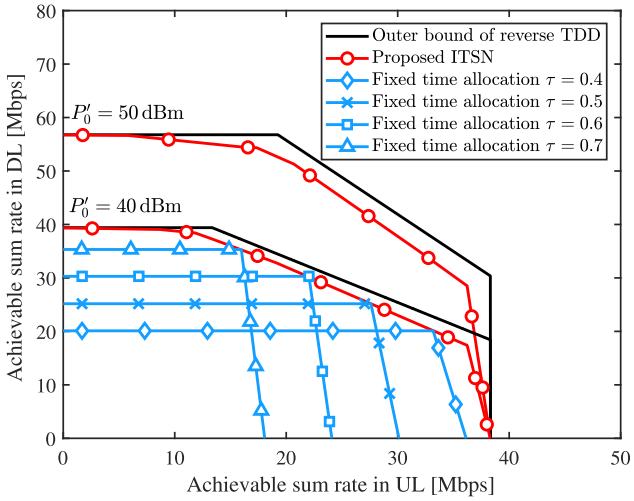

(a) Effect of the transmit power

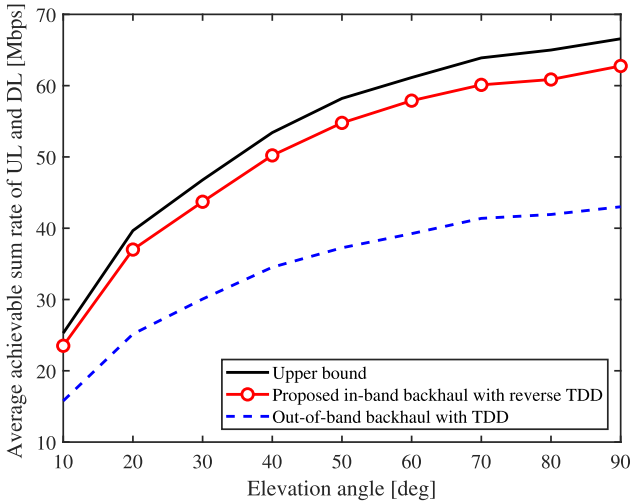

(b) Effect of the elevation angle: $\zeta = 0.5$, $P_0' = 50$ dBm.

Fig. 7. Performances for different powers and locations of the satellite: $M = 8 \times 2$, $P_{\mathrm{t}} = 35$ dBm, UMi scenario at 30 GHz.

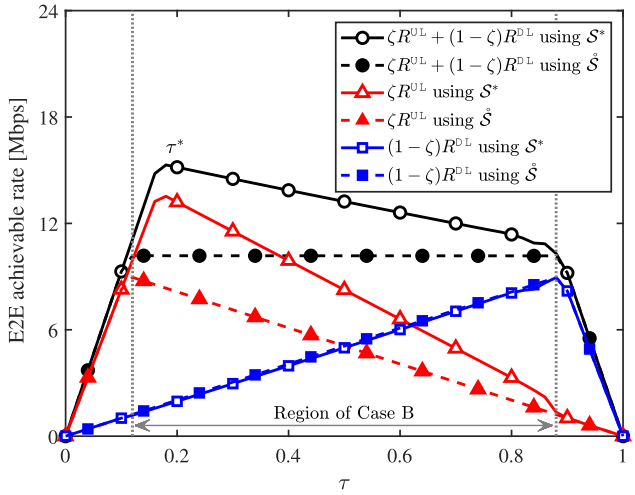

Fig. 8. An example of solving $\mathscr{P}_1(\tau)$ for discretized values of τ with the interval of 0.02. For this channel realization, the range of $0.12 \leqslant \tau \leqslant 0.88$ corresponds to Case B where $\mathscr{P}_{1,\mathrm{B}}(\tau)$ is solved for each τ. In this example, the optimal solution to $\mathscr{P}_0$ can be found at $\tau^* = 0.18$. The parameters are: $P_0' = 40$ dBm, $P_{\mathrm{t}} = 35$ dBm, $M = 8 \times 2$, and $\zeta = 0.4$.

DL, while achieving the similar maximum UL rate. Therefore, the use of a large array at the gNBs can be a power-efficient way to increase the UL-DL rate region. In particular, the impact of increasing M is more significant in the UMi scenario at 30 GHz than in the Rural scenario at 4 GHz.

Fig. 7 presents the effects of the satellite parameters on the achievable sum rate. Fig. 7(a) shows the effect of increasing the transmit power P_0'. We observe that the DL rate increases as P_0' increases, while the maximum achievable UL rate is almost unchanged by varying P_0'. This is because the transmit power of the satellite mainly affects the performance of the backhaul DL, and the interference to the access UL is negligible due to the BF at the gNBs. In addition, the advantage of joint optimization of τ and $\mathcal{S}$ in $\mathscr{P}_0$ is shown by comparing with a fixed time allocation scheme that solves $\mathscr{P}_1(\tau)$ for given τ. Fig. 7(b) shows the average achievable sum rate of UL and DL over 500 random channel realizations for different elevation angles of the satellite from the terrestrial origin. The average achievable sum rate increases with the elevation angle because the LOS probability increases while the propagation distance decreases. In particular, a significant improvement can be observed at low elevation angles, which can be verified by the behavior of the large-scale channel gains for different elevation angles in Fig. 4(c).

Fig. 8 shows the behaviors of the objective values in solving $\mathscr{P}_1(\tau)$ for a given channel realization according to given values of τ ranging from 0 to 1. In this example, the problem $\mathscr{P}_{1,\mathrm{B}}(\tau)$ is solved in the range of $0.12 \leqslant \tau \leqslant 0.88$ as the condition for Case B is met in Sec. III-C. After solving $\mathscr{P}_{1,\mathrm{B}}(\tau)$, the end-to-end UL rate R^{UL} increases from that of the initial result $\mathring{\mathcal{S}}$ while preserving the same end-to-end DL rate, which can be seen from the curves with triangle and square markers. We observe that the objective value, i.e., $\zeta R^{\mathrm{UL}} + (1-\zeta) R^{\mathrm{DL}}$, is improved by 50 % using the proposed solution $\mathcal{S}^*$ compared to the initial solution $\mathring{\mathcal{S}}$.

Fig. 9 shows the convergence behaviors of Algorithm 1 for random channel realizations. We see that the outer algorithm converges within around 10 iterations, and the inner algorithms converge within only a few iterations. These results indicate that the optimization variables converge to a stationary point by satisfying the necessary conditions.

VI. Conclusion

This paper proposed an in-band IAB architecture based on reverse TDD and gNB cooperation for next generation ITSNs with high spectral efficiency. The cooperative BF and resource allocation are jointly optimized for maximizing the weighted sum of end-to-end UL and DL rates. The constrained subproblems are formulated according to the proposed bilevel optimization framework, and an efficient algorithm is designed to satisfy the derived necessary conditions. Numerical results show that the proposed ITSN with in-band backhauling significantly outperforms the out-of-band backhauling. In addition, the achievable UL-DL rate region approaches the outer bound. The rate region can be more efficiently enlarged in both UL and DL by increasing the number of antennas at the gNBs than

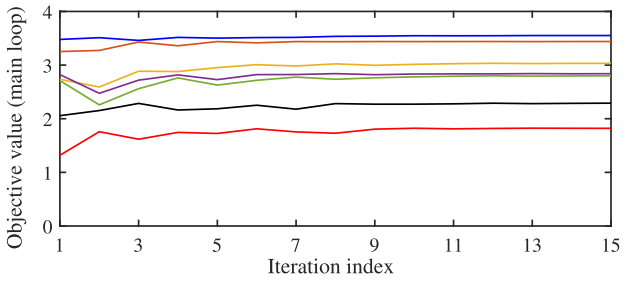

(a) Outer loop in lines 4–30

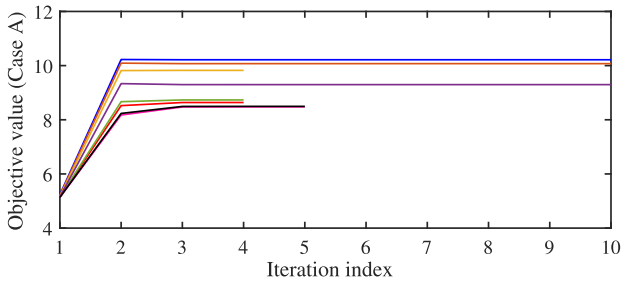

(b) Inner loop for Case A in lines 9–12

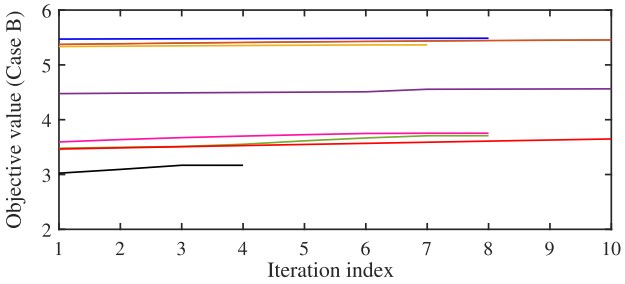

(c) Inner loop for Case B in lines 15–18

Fig. 9. Convergence behaviors of Algorithm 1. The sequences of the objective values are plotted for random channel realizations.

increasing the transmit power. The proposed TSN with in-band IAB can efficiently support the envisioned global broadband services with different traffic demands of UL and DL.

REFERENCES

[1] *Study on Using Satellite Access in 5G (Release 16)*, 3GPP, document TR 22.822, 2018.

[2] *Solutions for NR to Support Non-terrestrial Networks (NTN) (Release 16)*, 3GPP, document TR 38.821, 2023.

[3] X. Lin, S. Rommer, S. Euler, E. A. Yavuz, and R. S. Karlsson, "5G from space: An overview of 3GPP non-terrestrial networks," *IEEE Commun. Standards Mag.*, vol. 5, no. 4, pp. 147–153, Dec. 2021.

[4] F. Völk et al., "Field trial of a 5G non-terrestrial network using OpenAirInterface," *IEEE Open J. Veh. Technol.*, vol. 3, pp. 243–250, 2022.

[5] G. Kwon, W. Shin, A. Conti, W. C. Lindsey, and M. Z. Win, "Joint beamforming and resource allocation for integrated satellite-terrestrial networks," in *Proc. IEEE Int. Conf. Commun.*, Rome, Italy, May 2023, pp. 2147–2152.

[6] ITU-R Study Groups, *Draft New Recommendation ITU-R M.[IMT.FRAMEWORK FOR 2030 AND BEYOND]-Framework and Overall Objectives of the Future Development of IMT for 2030 and Beyond*, document ITU-R WP5D TD 905, 2023.

[7] T. Darwish, G. K. Kurt, H. Yanikomeroglu, M. Bellemare, and G. Lamontagne, "LEO satellites in 5G and beyond networks: A review from a standardization perspective," *IEEE Access*, vol. 10, pp. 35040–35060, 2022.

[8] T. Ahmmed, A. Alidadi, Z. Zhang, A. U. Chaudhry, and H. Yanikomeroglu, "The digital divide in Canada and the role of LEO satellites in bridging the gap," *IEEE Commun. Mag.*, vol. 60, no. 6, pp. 24–30, Jun. 2022.

[9] *Feasibility Study on New Services and Markets Technology Enablers—Network Operation (Release 15)*, 3GPP, document TR 22.864, 2016.

[10] R. De Gaudenzi, M. Luise, and L. Sanguinetti, "The open challenge of integrating satellites into (Beyond-) 5G cellular networks," *IEEE Netw.*, vol. 36, no. 2, pp. 168–174, Mar. 2022.

[11] R. De Gaudenzi, P. Angeletti, D. Petrolati, and E. Re, "Future technologies for very high throughput satellite systems," *Int. J. Satell. Commun. Netw.*, vol. 38, no. 2, pp. 141–161, Mar. 2020.

[12] M. M. Azari et al., "Evolution of non-terrestrial networks from 5G to 6G: A survey," *IEEE Commun. Surveys Tuts.*, vol. 24, no. 4, pp. 2633–2672, 4th Quart., 2022.

[13] S. Liu et al., "LEO satellite constellations for 5G and beyond: How will they reshape vertical domains?" *IEEE Commun. Mag.*, vol. 59, no. 7, pp. 30–36, Jul. 2021.

[14] D. Peng, A. Bandi, Y. Li, S. Chatzinotas, and B. Ottersten, "Hybrid beamforming, user scheduling, and resource allocation for integrated terrestrial-satellite communication," *IEEE Trans. Veh. Technol.*, vol. 70, no. 9, pp. 8868–8882, Sep. 2021.

[15] A. I. Perez-Neira, M. A. Vazquez, M. R. B. Shankar, S. Maleki, and S. Chatzinotas, "Signal processing for high-throughput satellites: Challenges in new interference-limited scenarios," *IEEE Signal Process. Mag.*, vol. 36, no. 4, pp. 112–131, Jul. 2019.

[16] D. Han, W. Liao, H. Peng, H. Wu, W. Wu, and X. Shen, "Joint cache placement and cooperative multicast beamforming in integrated satellite-terrestrial networks," *IEEE Trans. Veh. Technol.*, vol. 71, no. 3, pp. 3131–3143, Mar. 2022.

[17] M. K. Arti and M. R. Bhatnagar, "Beamforming and combining in hybrid satellite-terrestrial cooperative systems," *IEEE Commun. Lett.*, vol. 18, no. 3, pp. 483–486, Mar. 2014.

[18] W. Zeng, J. Zhang, D. W. K. Ng, B. Ai, and Z. Zhong, "Two-way hybrid terrestrial-satellite relaying systems: Performance analysis and relay selection," *IEEE Trans. Veh. Technol.*, vol. 68, no. 7, pp. 7011–7023, Jul. 2019.

[19] Q. Huang, M. Lin, J.-B. Wang, T. A. Tsiftsis, and J. Wang, "Energy efficient beamforming schemes for satellite-aerial-terrestrial networks," *IEEE Trans. Commun.*, vol. 68, no. 6, pp. 3863–3875, Jun. 2020.

[20] M. Toka, M. Vaezi, and W. Shin, "Outage analysis of alamouti-NOMA scheme for hybrid satellite–terrestrial relay networks," *IEEE Internet Things J.*, vol. 10, no. 6, pp. 5293–5303, Mar. 2023.

[21] X. Zhu, C. Jiang, L. Kuang, N. Ge, and J. Lu, "Non-orthogonal multiple access based integrated terrestrial-satellite networks," *IEEE J. Sel. Areas Commun.*, vol. 35, no. 10, pp. 2253–2267, Oct. 2017.

[22] J. Chu and X. Chen, "Robust design for integrated satellite-terrestrial Internet of Things," *IEEE Internet Things J.*, vol. 8, no. 11, pp. 9072–9083, Jun. 2021.

[23] H. Dong, C. Hua, L. Liu, W. Xu, S. Guo, and R. Tafazolli, "Joint beamformer design and user scheduling for integrated terrestrial-satellite networks," *IEEE Trans. Wireless Commun.*, vol. 22, no. 10, pp. 6398–6414, Oct. 2023.

[24] L. Yin and B. Clerckx, "Rate-splitting multiple access for satellite-terrestrial integrated networks: Benefits of coordination and cooperation," *IEEE Trans. Wireless Commun.*, vol. 22, no. 1, pp. 317–332, Jan. 2023.

[25] J. Lee, J. Lee, L. Yin, W. Shin, and B. Clerckx, "Coordinated rate-splitting multiple access for integrated satellite-terrestrial networks with super-common message," *IEEE Trans. Veh. Technol.*, vol. 73, no. 2, pp. 2989–2994, Feb. 2024.

[26] X. Zhu, C. Jiang, L. Yin, L. Kuang, N. Ge, and J. Lu, "Cooperative multigroup multicast transmission in integrated terrestrial-satellite networks," *IEEE J. Sel. Areas Commun.*, vol. 36, no. 5, pp. 981–992, May 2018.

[27] H. Dong, C. Hua, L. Liu, W. Xu, and R. Tafazolli, "Intelligent reflecting surface-aided integrated terrestrial-satellite networks," *IEEE Trans. Wireless Commun.*, vol. 22, no. 4, pp. 2507–2522, Apr. 2023.

[28] X. Artiga et al., "Shared access satellite-terrestrial reconfigurable backhaul network enabled by smart antennas at mmWave band," *IEEE Netw.*, vol. 32, no. 5, pp. 46–53, Sep. 2018.

[29] X. Zhu and C. Jiang, "Integrated satellite-terrestrial networks toward 6G: Architectures, applications, and challenges," *IEEE Internet Things J.*, vol. 9, no. 1, pp. 437–461, Jan. 2022.

[30] Y. Zhang, M. A. Kishk, and M.-S. Alouini, "A survey on integrated access and backhaul networks," *Frontiers Commun. Netw.*, vol. 2, pp. 1–24, Jun. 2021.

[31] M. Shaat, E. Lagunas, A. I. Perez-Neira, and S. Chatzinotas, "Integrated terrestrial-satellite wireless backhauling: Resource management and benefits for 5G," *IEEE Veh. Technol. Mag.*, vol. 13, no. 3, pp. 39–47, Sep. 2018.

[32] Y. Turk and E. Zeydan, "Satellite backhauling for next generation cellular networks: Challenges and opportunities," *IEEE Commun. Mag.*, vol. 57, no. 12, pp. 52–57, Dec. 2019.

[33] J. J. Spilker Jr., *Digital Communications by Satellite*. Upper Saddle River, NJ, USA: Prentice-Hall, 1977.

[34] W. C. Lindsey and M. K. Simon, *Telecommunication Systems Engineering*. Upper Saddle River, NJ, USA: Prentice-Hall, 1973.

[35] *NR; Integrated Access and Backhaul Radio Transmission and Reception (Release 17)*, 3GPP, document TS 38.174, 2022.

[36] N. Wang, E. Hossain, and V. K. Bhargava, "Joint downlink cell association and bandwidth allocation for wireless backhauling in two-tier HetNets with large-scale antenna arrays," *IEEE Trans. Wireless Commun.*, vol. 15, no. 5, pp. 3251–3268, May 2016.

[37] J. Niu, G. Y. Li, Y. Li, D. Fang, and X. Li, "Joint 3D beamforming and resource allocation for small cell wireless backhaul in HetNets," *IEEE Commun. Lett.*, vol. 21, no. 10, pp. 2286–2289, Oct. 2017.

[38] T. M. Nguyen, A. Yadav, W. Ajib, and C. Assi, "Resource allocation in two-tier wireless backhaul heterogeneous networks," *IEEE Trans. Wireless Commun.*, vol. 15, no. 10, pp. 6690–6704, Oct. 2016.

[39] H. Zhang, H. Liu, J. Cheng, and V. C. M. Leung, "Downlink energy efficiency of power allocation and wireless backhaul bandwidth allocation in heterogeneous small cell networks," *IEEE Trans. Commun.*, vol. 66, no. 4, pp. 1705–1716, Apr. 2018.

[40] L. Sanguinetti, A. L. Moustakas, and M. Debbah, "Interference management in 5G reverse TDD HetNets with wireless backhaul: A large system analysis," *IEEE J. Sel. Areas Commun.*, vol. 33, no. 6, pp. 1187–1200, Jun. 2015.

[41] T. M. Nguyen, A. Yadav, W. Ajib, and C. Assi, "Centralized and distributed energy efficiency designs in wireless backhaul HetNets," *IEEE Trans. Wireless Commun.*, vol. 16, no. 7, pp. 4711–4726, Jul. 2017.

[42] G. Kwon and H. Park, "Joint user association and beamforming design for millimeter wave UDN with wireless backhaul," *IEEE J. Sel. Areas Commun.*, vol. 37, no. 12, pp. 2653–2668, Dec. 2019.

[43] B. Li, D. Zhu, and P. Liang, "Small cell in-band wireless backhaul in massive MIMO systems: A cooperation of next-generation techniques," *IEEE Trans. Wireless Commun.*, vol. 14, no. 12, pp. 7057–7069, Dec. 2015.

[44] G. Kwon and H. Park, "Beamforming design for low-power in-band wireless backhaul systems: Centralized and distributed approaches," *IEEE Trans. Veh. Technol.*, vol. 68, no. 2, pp. 1549–1563, Feb. 2019.

[45] A. Adhikary, H. S. Dhillon, and G. Caire, "Massive-MIMO meets HetNet: Interference coordination through spatial blanking," *IEEE J. Sel. Areas Commun.*, vol. 33, no. 6, pp. 1171–1186, Jun. 2015.

[46] T. K. Vu, M. Bennis, S. Samarakoon, M. Debbah, and M. Latva-Aho, "Joint load balancing and interference mitigation in 5G heterogeneous networks," *IEEE Trans. Wireless Commun.*, vol. 16, no. 9, pp. 6032–6046, Sep. 2017.

[47] L. You, K.-X. Li, J. Wang, X. Gao, X.-G. Xia, and B. Ottersten, "Massive MIMO transmission for LEO satellite communications," *IEEE J. Sel. Areas Commun.*, vol. 38, no. 8, pp. 1851–1865, Aug. 2020.

[48] K.-X. Li et al., "Downlink transmit design for massive MIMO LEO satellite communications," *IEEE Trans. Commun.*, vol. 70, no. 2, pp. 1014–1028, Feb. 2022.

[49] Y. Yan, K. An, B. Zhang, S. Li, and D. Guo, "Outage constrained robust beamforming for multicast multibeam satellite systems with a phase error," *IEEE Trans. Aerosp. Electron. Syst.*, vol. 56, no. 5, pp. 4152–4156, Oct. 2020.

[50] M. A. Vázquez, L. Blanco, and A. I. Pérez-Neira, "Spectrum sharing backhaul satellite-terrestrial systems via analog beamforming," *IEEE J. Sel. Topics Signal Process.*, vol. 12, no. 2, pp. 270–281, May 2018.

[51] B. Deng, C. Jiang, J. Yan, N. Ge, S. Guo, and S. Zhao, "Joint multi-group precoding and resource allocation in integrated terrestrial-satellite networks," *IEEE Trans. Veh. Technol.*, vol. 68, no. 8, pp. 8075–8090, Aug. 2019.

[52] M. Lin, Z. Lin, W.-P. Zhu, and J.-B. Wang, "Joint beamforming for secure communication in cognitive satellite terrestrial networks," *IEEE J. Sel. Areas Commun.*, vol. 36, no. 5, pp. 1017–1029, May 2018.

[53] Y. Zhang, L. Yin, C. Jiang, and Y. Qian, "Joint beamforming design and resource allocation for terrestrial-satellite cooperation system," *IEEE Trans. Commun.*, vol. 68, no. 2, pp. 778–791, Feb. 2020.

[54] Z. Lin, M. Lin, J.-B. Wang, Y. Huang, and W.-P. Zhu, "Robust secure beamforming for 5G cellular networks coexisting with satellite networks," *IEEE J. Sel. Areas Commun.*, vol. 36, no. 4, pp. 932–945, Apr. 2018.

[55] Q. Wang, H. Zhang, J.-B. Wang, F. Yang, and G. Y. Li, "Joint beamforming for integrated mmWave satellite-terrestrial self-backhauled networks," *IEEE Trans. Veh. Technol.*, vol. 70, no. 9, pp. 9103–9117, Sep. 2021.

[56] A. Bletsas, H. Shin, and M. Z. Win, "Cooperative communications with outage-optimal opportunistic relaying," *IEEE Trans. Wireless Commun.*, vol. 6, no. 9, pp. 3450–3460, Sep. 2007.

[57] A. F. Molisch, M. V. Clark, H. Dai, M. Z. Win, and J. H. Winters, "Method and apparatus for reducing interference in multiple-input-multiple-output (MIMO) systems," U.S. Patent 7 912 014, Mar. 22, 2011.

[58] Y. Zhang, A. Liu, P. Li, and S. Jiang, "Deep learning (DL)-based channel prediction and hybrid beamforming for LEO satellite massive MIMO system," *IEEE Internet Things J.*, vol. 9, no. 23, pp. 23705–23715, Dec. 2022.

[59] Y. Zhang, Y. Wu, A. Liu, X. Xia, T. Pan, and X. Liu, "Deep learning-based channel prediction for LEO satellite massive MIMO communication system," *IEEE Wireless Commun. Lett.*, vol. 10, no. 8, pp. 1835–1839, Aug. 2021.

[60] B. Zheng, S. Lin, and R. Zhang, "Intelligent reflecting surface-aided LEO satellite communication: Cooperative passive beamforming and distributed channel estimation," *IEEE J. Sel. Areas Commun.*, vol. 40, no. 10, pp. 3057–3070, Oct. 2022.

[61] H. Ji, J. Cho, Y. Kim, J. Han, J. Lee, and S. Choi, "Flexible time division duplex method and apparatus for communication system," U.S. Patent 9 906 293 B2, Sep. 27, 2018.

[62] *NR; Physical Layer Procedures for Control (Release 17)*, 3GPP, document TS 38.213, 2022.

[63] A. P. Hulbert and K. D. Tomkinson, "Method of communication in a time division duplex (TDD) satellite communication system," U.S. Patent 20 070 274 249 A1, Feb. 29, 2007.

[64] P.-D. Arapoglou, K. Liolis, M. Bertinelli, A. Panagopoulos, P. Cottis, and R. De Gaudenzi, "MIMO over satellite: A review," *IEEE Commun. Surveys Tuts.*, vol. 13, no. 1, pp. 27–51, 1st Quart., 2011.

[65] *Study on New Radio (NR) to Support Non-Terrestrial Networks (Release 15)*, 3GPP, document TR 38.811, 2020.

[66] *Study on Channel Model for Frequencies From 0.5 to 100 GHz (Release 16)*, 3GPP, document TR 38.901, 2019.

[67] G. Torsoli, M. Z. Win, and A. Conti, "Blockage intelligence in complex environments for beyond 5G localization," *IEEE J. Sel. Areas Commun.*, vol. 41, no. 6, pp. 1688–1701, Jun. 2023.

[68] A. Conti, W. M. Gifford, M. Z. Win, and M. Chiani, "Optimized simple bounds for diversity systems," *IEEE Trans. Commun.*, vol. 57, no. 9, pp. 2674–2685, Sep. 2009.

[69] W. M. Gifford, A. Conti, M. Chiani, and M. Z. Win, "On the SNR penalties of ideal and non-ideal subset diversity systems," *IEEE Trans. Inf. Theory*, vol. 58, no. 6, pp. 3708–3724, Jun. 2012.

[70] A. Conti, M. Z. Win, and M. Chiani, "Slow adaptive M-QAM with diversity in fast fading and shadowing," *IEEE Trans. Commun.*, vol. 55, no. 5, pp. 895–905, May 2007.

[71] J. H. Winters, Y.-S. Choi, B.-J. J. Kim, A. F. Molisch, M. Z. Win, and H. Luo, "Method of selecting receive antennas for MIMO systems," U.S. Patent 7 006 810, Feb. 28, 2006.

[72] M. Z. Win and J. H. Winters, "Methods and systems for spatial processing," U.S. Patent 6 804 312, Oct. 12, 2004.

[73] U. Siddique, H. Tabassum, and E. Hossain, "Downlink spectrum allocation for in-band and out-band wireless backhauling of full-duplex small cells," *IEEE Trans. Commun.*, vol. 65, no. 8, pp. 3538–3554, Aug. 2017.

[74] A. Bonfante et al., "5G massive MIMO architectures: Self-backhauled small cells versus direct access," *IEEE Trans. Veh. Technol.*, vol. 68, no. 10, pp. 10003–10017, Oct. 2019.

[75] G. Golub and C. V. Loan, *Matrix Computations*, 3rd ed. Baltimore, MD, USA: The Johns Hopkins Univ. Press, 1996.

[76] J. Kim, H.-W. Lee, and S. Chong, "Virtual cell beamforming in cooperative networks," *IEEE J. Sel. Areas Commun.*, vol. 32, no. 6, pp. 1126–1138, Jun. 2014.

[77] A. Sinha, P. Malo, and K. Deb, "A review on bilevel optimization: From classical to evolutionary approaches and applications," *IEEE Trans. Evol. Comput.*, vol. 22, no. 2, pp. 276–295, Apr. 2018.

[78] W. H. Hesselink. (Jul. 2003). *Ternary Search*. [Online]. Available: http://wimhesselink.nl/pub/whh303.pdf

[79] D. P. Bertsekas, *Nonlinear Programming*, 3rd ed. Belmont, MA, USA: Athena Sci., 2016.

Girim Kwon (Member, IEEE) received the B.S. degree (with the highest honor) in electrical engineering from the University of Seoul, Seoul, South Korea, in 2013, and the M.S. and Ph.D. degrees in electrical engineering from Korea Advanced Institute of Science and Technology (KAIST), Daejeon, South Korea, in 2014 and 2020, respectively.

He is currently a Postdoctoral Fellow with the Wireless Information and Network Sciences Laboratory at the Massachusetts Institute of Technology, Cambridge, MA, USA. His current research interests include wireless communications, network localization and navigation, satellite networks, and machine learning.

Dr. Kwon was a recipient of the S-Oil Best Dissertation Award in 2021, the Best Ph.D. Dissertation Award from KAIST in 2020, the ICT Paper Award from the Electronic Times in 2018, and the Global Ph.D. Fellowship from the Korean Government in 2015.

Wonjae Shin (Senior Member, IEEE) received the Ph.D. degree from the Department of Electrical and Computer Engineering, Seoul National University (SNU), South Korea, in 2017. From 2007 to 2014, he was a member of the Technical Staff with the Samsung Advanced Institute of Technology and Samsung Electronics Company Ltd., South Korea, where he contributed to next-generation wireless communication networks, especially for 3GPP LTE/LTE-advanced standardizations. From 2016 to 2018, he was a Visiting Scholar and a Postdoctoral Research Fellow with Princeton University, Princeton, NJ, USA. Since 2023, he has been with the School of Electrical Engineering, Korea University, Seoul, South Korea, where he is currently an Associate Professor. Prior to joining Korea University, he was a Faculty Member with Pusan National University, Busan, and Ajou University, Suwon, South Korea. His research interests include the design and analysis of future wireless communication systems, such as interference-limited networks and machine learning for wireless networks.

Dr. Shin was a recipient of the Fred W. Ellersick Prize and the Asia-Pacific Outstanding Young Researcher Award from the IEEE Communications Society in 2020, the International Conference on ICT Convergence (ICTC) Best Workshop Paper Award in 2022, the JOURNAL OF KOREAN INSTITUTE OF COMMUNICATIONS AND INFORMATION SCIENCES Best Paper Award in 2021, the Best Ph.D. Dissertation Award from SNU in 2017, the Gold Prize from the IEEE Student Paper Contest (Seoul Section) in 2014, and the Award of the Ministry of Science and ICT of Korea in IDIS-Electronic News ICT Paper Contest in 2017. He is an Associate Editor of the IEEE OPEN JOURNAL OF COMMUNICATIONS SOCIETY.

Andrea Conti (Fellow, IEEE) is a Professor and founding director of the Wireless Communication and Localization Networks Laboratory at the University of Ferrara, Italy. Prior to joining the University of Ferrara, he was with CNIT and with IEIIT-CNR.

In Summer 2001, he was with the Wireless Systems Research Department at AT&T Research Laboratories. Since 2003, he has been a frequent Visitor with the Wireless Information and Network Sciences Laboratory at the Massachusetts Institute of Technology, where he presently holds the Research Affiliate appointment. His research interests involve the theory and experimentation of wireless communication and localization systems. His current research topics include network localization and navigation, distributed sensing, adaptive diversity communications, and quantum information science.

Dr. Conti has served as editor for IEEE journals and chaired international conferences. He was elected Chair of the IEEE Communications Society's Radio Communications Technical Committee and is Co-founder of the IEEE Quantum Communications and Information Technology Emerging Technical Subcommittee. He received the HTE Puskás Tivadar Medal, the IEEE Communications Society's Fred W. Ellersick Prize, and the IEEE Communications Society's Stephen O. Rice Prize in the field of Communications Theory. He is an elected Fellow of the IET and a member of Sigma Xi. He has been selected as an IEEE Distinguished Lecturer.

William C. Lindsey (Life Fellow, IEEE) received the Ph.D. degree in electrical engineering from Purdue University in 1962. He was the Supervisor of the Communications Research Group at Caltech's Jet Propulsion Laboratory (1962–1968), and the Founder, the CEO, and the President of LinCom Corporation (1972–2000). He joined the University of Southern California in 1968.

He is an internationally known expert with over 50 years of experience in the field of Communication Sciences. He authored three landmark systems engineering books on the subject of modulation-coding, demodulation-decoding, data detection, synchronization, and tracking for communication technology applications. His patents have been implemented in numerous communication satellite systems, ground stations, and mobile communications receivers located around the world.

Dr. Lindsey's synchronization and communications research has spearheaded the digital communications revolution, and it has created novel technologies for space and mobile wireless communications. His digital-data transition-tracking loop (DTTL) enabled the decoding of the first photos of Mars from NASA's Mariner spacecraft as well as images from the Voyager missions, and it was critical to Space Shuttle and space station communications efforts. It also led to the concept of "digital phase-locked systems on a chip" used in modern mobile radios and localization systems. He was one of the pioneering founders of the IEEE Communications Society. He was honored with the IEEE Third Millennium Medal in 2000 and the prestigious IEEE Eric E. Sumner Award in 2017. He is a member of the National Academy of Engineering.

Moe Z. Win (Fellow, IEEE) is a Professor at the Massachusetts Institute of Technology (MIT) and the founding director of the Wireless Information and Network Sciences Laboratory. Prior to joining MIT, he was with AT&T Research Laboratories and with NASA Jet Propulsion Laboratory.

His research encompasses fundamental theories, algorithm design, and network experimentation for a broad range of real-world problems. His current research topics include ultra-wideband systems, network localization and navigation, network interference exploitation, and quantum information science. He has served the IEEE Communications Society as an elected Member-at-Large on the Board of Governors, as elected Chair of the Radio Communications Committee, and as an IEEE Distinguished Lecturer. Over the last two decades, he held various editorial positions for IEEE journals and organized numerous international conferences. Recently, he served on the SIAM Diversity Advisory Committee.

Dr. Win is an elected Fellow of the AAAS, the EURASIP, and the IET. He was honored with two IEEE Technical Field Awards: the IEEE Kiyo Tomiyasu Award (2011) and the IEEE Eric E. Sumner Award (2006, jointly with R. A. Scholtz). His publications, co-authored with students and colleagues, have received several awards. Other recognitions include the MIT Everett Moore Baker Award (2022), the IEEE Vehicular Technology Society James Evans Avant Garde Award (2022), the IEEE Communications Society Edwin H. Armstrong Achievement Award (2016), the Cristoforo Colombo International Prize for Communications (2013), the Copernicus Fellowship (2011) and the *Laurea Honoris Causa* (2008) both from the Università degli Studi di Ferrara, and the U.S. Presidential Early Career Award for Scientists and Engineers (2004).